



Research article

A novel VEGFR inhibitor ZLF-095 with potent antitumor activity and low toxicity

Xiao Li ^{a,1}, Jia Wang ^{a,1}, Qianqian Wang ^{a,1}, Tianwen Luo ^{a,1}, Xuejiao Song ^b, Guoquan Wan ^a, Zhanzhan Feng ^a, Xiaojie He ^a, Qian Lei ^c, Ying Xu ^d, Xinyu You ^e, Luoting Yu ^{a,*}, Lidan Zhang ^{f,**}, Lifeng Zhao ^{g,***}

^a State Key Laboratory of Biotherapy/Collaborative Innovation Center for Biotherapy, West China Hospital, West China Medical School, Sichuan University, Chengdu, 610041, China

^b West China School of Public Health and West China Fourth Hospital, Sichuan University, 610000, China

^c Targeted Tracer Research and Development Laboratory, Precision Medicine Key Laboratory of Sichuan Province & Precision Medicine Center, West China Hospital, Sichuan University, Chengdu, Sichuan, 610093, China

^d School of Chemical Engineering, Northwest University, No.229 North Taibai Road, Xi'an, Shaanxi, 710069, China

^e College of Chemistry and Pharmaceutical Engineering, Huanghuai University, Zhumadian 463000, China

^f Laboratory of Anesthesia and Critical Care Medicine, National-Local Joint Engineering Research Centre of Translational Medicine of Anesthesiology, West China Hospital, Sichuan University, China

^g Sichuan Industrial Institute of Antibiotics, School of Pharmacy, Chengdu University, Chengdu, 610106, China

ARTICLE INFO

Keywords:

Antiangiogenic
Cancer
ROS
Mitochondrial membrane potential
Pyroptosis

ABSTRACT

Angiogenesis plays a critical role in the survival, progression and metastasis of malignant tumors. Multiple factors are known to induce tumor angiogenesis, vascular endothelial growth factor (VEGF) is the most important one. Lenvatinib is an oral multi-kinase inhibitor of VEGFRs which has been approved for the treatment of various malignancies as the first-line agent by the Food and Drug Administration (FDA). It shows excellent antitumor efficacy in clinical practice. However, the adverse effects of Lenvatinib may seriously impair the therapeutic effect. Here we report the discovery and characterization of a novel VEGFR inhibitor (ZLF-095), which exhibited high activity and selectivity for VEGFR1/2/3. ZLF-095 displayed apparently antitumor effect in vitro and in vivo. We discovered that Lenvatinib could provoke fulminant ROS-caspase3-GSDME-dependent pyroptosis in GSDME-expressing cells by loss of mitochondrial membrane potential, which may be one of the reasons for Lenvatinib's toxicity. Meanwhile, ZLF-095 showed less toxicity than Lenvatinib by switching pyroptosis to apoptosis. These results suggest that ZLF-095 could become a potential angiogenesis inhibitor for cancer therapy.

1. Introduction

Since Judah Folkman hypothesized in 1971 that angiogenesis is required for the growth of solid tumors [1], numerous studies have

* Corresponding author.

** Corresponding author.

*** Corresponding author.

E-mail addresses: yuluot@scu.edu.cn (L. Yu), zhanglidan0510@wchscu.cn (L. Zhang), lifengzhao@cdu.edu.cn (L. Zhao).

¹ Co-first authors.

<https://doi.org/10.1016/j.heliyon.2023.e15152>

Received 14 December 2022; Received in revised form 23 March 2023; Accepted 28 March 2023

Available online 19 April 2023

2405-8440/© 2023 Published by Elsevier Ltd.

This is an open access article under the CC BY-NC-ND license

(<http://creativecommons.org/licenses/by-nc-nd/4.0/>).

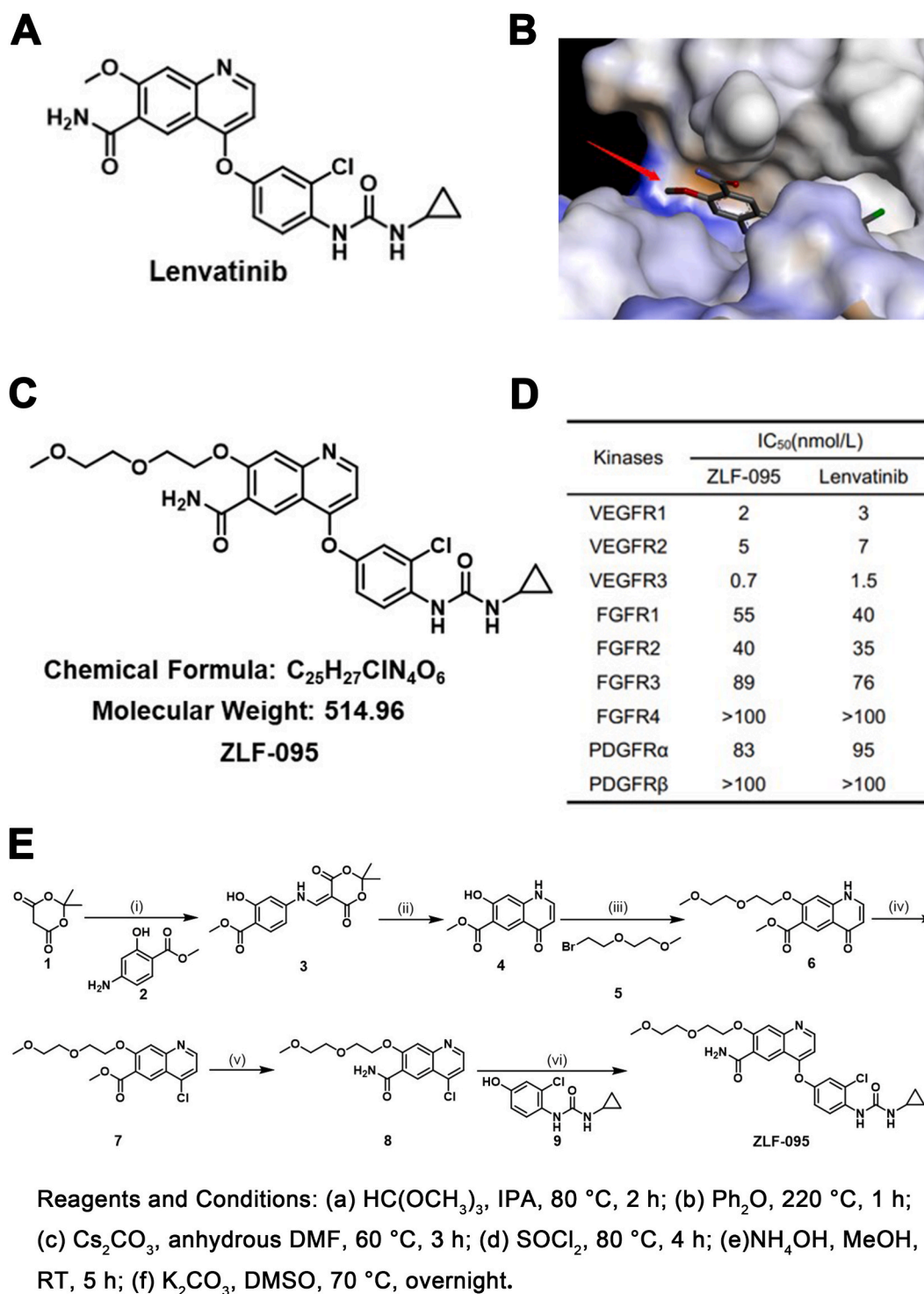


Fig. 1. Identification of ZLF-095. (A) Chemical structures of Lenvatinib. (B) Crystal structure of Lenvatinib bound to the VEGFR2 catalytic domain (PDB ID: 3WZD). The red arrow refers to possible linker-tethering positions. (C) Chemical structures of ZLF-095. (D) IC₅₀ values of ZLF-095 and Lenvatinib against a panel of kinases. (E) The synthetic route of compound ZLF-095.

identified that angiogenesis plays a critical role in the survival, progression, and metastasis of malignant tumors [2–5]. Neo-vascularization is widely distributed in the tumor stroma, which is characterized by large number, random distribution, irregular lumen and abundant connection with arteriovenous [6–8]. This resulted in improving the tumor blood supply, providing adequate

nutrition for occurrence and development of cancer. In addition, the basement membranes of the neovascularization endothelial cells are discontinuous or completely absent, which led to entry of tumor cells into the circulation easily due to uncontrolled vascular permeability, eventually leading to tumor metastasis [2].

Multiple factors are known to induce tumor angiogenesis. Vascular endothelial growth factor (VEGF) is the most important one which was discovered by Ferrara et al., in 1989 [7, 9, 10]. The binding of VEGF and its receptor VEGFR (vascular endothelial growth factor receptor) activates downstream signaling cascades including PI3K/Akt, p38/MAPK and RAF/MEK/ERK, etc [11]. These actions directly regulate endothelial survival, migration, proliferation and thus promote neovascularization. VEGF/VEGFR also promotes angiogenesis by recruiting tumor-associated macrophages (TAMs) to tumor microenvironment, which support angiogenesis through the release of proteases, cytokines, and various growth factors [12–14].

Because of these direct and indirect proangiogenic activities of VEGFR and interrelated signaling pathways, they become the targets of many first-line anti-cancer drugs, such as Lenvatinib, pazopanib, sunitinib and bevacizumab [15–20]. Lenvatinib is an oral multi-kinase inhibitor of VEGFRs, FGFR 1–4, PDGFR α , RET and KIT developed by Eisai. It has been approved for the treatment of thyroid cancer (THCA), renal cell carcinoma (RCC) and advanced hepatocellular carcinoma (HCC) as the first-line systemic therapeutic agent by FDA [21–23]. Lenvatinib shows excellent antitumor efficacy in clinical practice, significantly prolongs the overall survival of patients. However, adverse effects of Lenvatinib are frequent in clinical applications, including fatigue, nausea, vomiting, hypertension and diarrhea, even trigger liver injury, heart failure and thrombosis [24–26]. These common adverse events of Lenvatinib are often responsible for dose reductions or treatment interruptions, which might seriously impair the therapeutic effect to cause therapeutic failure.

With the aim of improving the therapeutic efficacy and reducing the toxic side effects of Lenvatinib in the treatment of cancer, we carried out the current study. We have set up a compound library of Lenvatinib analogues. Potent Compound ZLF-095 from the self-built compound library was chosen for further studies by screening of kinase activity and antitumor activity in vitro. ZLF-095 significantly suppressed angiogenesis by inhibiting the VEGF/VEGFR2 and their downstream signaling pathway. Meanwhile, it exhibited apparently antitumor effect and antimetastatic potency in vitro and in vivo. More importantly, ZLF-095 displayed lower toxicity than Lenvatinib. We found that fulminant pyroptosis was induced by Lenvatinib in normal liver cells LO2, HCC cells (HepG2 and Hepa3B2.1-7) and CC cells (HCT116). Cell and molecular biological experiments validated Lenvatinib could provoke ROS-caspase3-GSDME-dependent pyroptosis in GSDME-expressing cells by loss of mitochondrial membrane potential ($\Delta\Psi_m$). Pyroptosis could induce rapid cell-membrane rupture and the release of intracellular contents, resulting in fever, hepatotoxicity, septicemia and other serious symptoms [27–29]. And it might be one of the reasons for the toxicity of Lenvatinib. In comparison, ZLF-095 had no effect on mitochondrial membrane potential and therefore switched pyroptosis to apoptosis, thus successfully avoiding unwanted side effects. Our results suggest that ZLF-095 might become a potential angiogenesis inhibitor for tumor therapy.

2. Materials and methods

2.1. Synthesis of ZLF-095

The synthetic route of the compound ZLF-095 was shown in Fig. 1E.

Step i: *methyl 4-((2,2-dimethyl-4,6-dioxo-1,3-dioxan-5-ylidene)methyl)amino-2-hydroxy benzoate* (3). The mixture of 2,2-dimethyl-1,3-dioxane-4,6-dione (1) (5 g, 34.7 mmol) and trimethyl orthoformate (4.8 g, 45.1 mmol) in isopropyl alcohol (100 mL) was stirred at 80 °C for 1 h. Then 3-Hydroxy-4-(methoxycarbonyl)aniline (2) (4.6 g, 27.8 mmol) was added, and the reaction was left to proceed for 1 h. When the reaction was completed, the reaction mixture was cooled to room temperature, filtrated and washed with acetaldehyde to obtain a yellow solid (9.9 g, 89%). ¹H NMR (400 MHz, Chloroform-*d*) δ 12.13 (s, 1H), 8.57 (s, 1H), 7.79 (m, 1H), 7.13 (s, 1H), 5.79 (d, *J* = 4.1 Hz, 1H), 3.72 (s, 1H), 3.66 (s, 3H), 1.71 (s, 6H).

Step ii: *methyl 7-hydroxy-4-oxo-1,4-dihydroquinoline-6-carboxylate* (4). To a solution of diphenyl ether (40 mL) was added compound 3 (9.2 g, 28.6 mmol) and the mixture was stirred at 220 °C for 1 h. When the reaction was completed, the reaction mixture was cooled to room temperature, added diethyl ether (15 mL), stirred for 0.5 h, filtrated and washed with acetaldehyde to obtain a yellow solid (5.1 g, 81%). ¹H NMR (400 MHz, Chloroform-*d*) δ 8.77 (d, *J* = 4.5 Hz, 1H), 8.63 (s, 1H), 7.80 (s, 1H), 7.65 (d, *J* = 4.1 Hz, 1H), 7.60 (s, 1H), 7.60 (s, 1H), 4.10 (s, 3H).

Step iii: *methyl 7-(2-(2-methoxyethoxy)ethoxy)-4-oxo-1,4-dihydroquinoline-6-carboxylate* (6). To a solution of compound 4 (5 g, 22.8 mmol) and cesium carbonate (14.8 g, 45.6 mmol) in dry DMF (50 mL) was added 1-bromo-2-(2-methoxyethoxy)ethane (5) (8.3 g, 45.6 mmol), the reaction mixture was stirred at 60 °C for 3 h. When the reaction was completed, the solution was poured into ice water, extracted with ethyl acetate. The organic phase was concentrated under vacuum, to obtain the crude product, purified by column chromatography to give 4 as a yellow solid (6.4 g, 88%). ¹H NMR (400 MHz, Chloroform-*d*) δ 8.87 (d, *J* = 4.3 Hz, 1H), 7.63 (s, 1H), 7.40 (s, 1H), 7.21 (d, *J* = 2.1 Hz, 1H), 7.11 (d, *J* = 1.3 Hz, 1H), 3.78 (s, 3H), 3.67–3.59 (m, 8H), 3.37 (s, 3H).

Step iv: *methyl 4-chloro-7-(2-(2-methoxyethoxy)ethoxy)quinoline-6-carboxylate* (7). A mixture of compound 6 (5 g, 15.6 mmol), thionyl chloride (50 mL) and DMF (1 mL) was heated to 80 °C and stirred for 4 h. When the reaction was completed, the solution was concentrated under vacuum, sodium bicarbonate solution was added to the crude product and stirred until no gas was produced, filtrated to obtain a yellow solid (6.1 g, 69%). ¹H NMR (400 MHz, Chloroform-*d*) δ 7.69 (s, 1H), 7.30 (s, 1H), 7.25 (d, *J* = 2.5 Hz, 1H), 7.09 (d, *J* = 1.3 Hz, 1H), 3.85 (s, 3H), 3.58–3.51 (m, 8H), 3.31 (s, 3H).

Step v: *4-chloro-7-(2-(2-methoxyethoxy)ethoxy)quinoline-6-carboxamide* (8). The mixture of compound 7 (5 g, 14.7 mmol), methanol (60 mL) and ammonium hydroxide (60 mL) was stirred at room temperature for 5 h. When the reaction was completed, the reaction mixture was filtrated and washed with water to obtain a yellow solid (3.3 g, 69%). ¹H NMR (400 MHz, Chloroform-*d*) δ 9.12 (s, 2H),

87.59 (s, 1H), 7.32 (s, 1H), 7.16 (d, $J = 2.5$ Hz, 1H), 7.12 (d, $J = 1.3$ Hz, 1H), 3.56–3.50 (m, 8H), 3.44 (s, 3H).

Step vi: 4-(3-chloro-4-(3-cyclopropylureido)phenoxy)-7-(2-(2-methoxyethoxy)ethoxy)quinoline-6-carboxamide (ZLF-095). To a solution of compound 8 (2 g, 6.1 mmol), potassium carbonate (1.7 g, 12.2 mmol) in dimethyl sulfoxide (20 mL) was added 1-(2-chloro-4-hydroxyphenyl)-3-cyclopropylurea (9) (2.1 g, 9.2 mmol). The reaction mixture was stirred at 70 °C overnight. When the reaction was completed, the reaction mixture was cooled to room temperature, added water (40 mL) and acetone (20 mL), stirred for 0.5 h, filtrated and washed with water to obtain the crude product, purified by column chromatography to give ZLF-095 as a yellow solid (1.5 g, 48%). ¹H NMR (400 MHz, Chloroform-*d*) δ 9.26 (s, 1H), 8.65 (s, 1H), 8.41 (d, $J = 8.8$ Hz, 1H), 8.17 (s, 1H), 7.74 (s, 1H), 7.61 (s, 1H), 7.23 (d, $J = 2.8$ Hz, 1H), δ 7.10 (dd, $J = 2.8, 2.4$ Hz, 1H), δ 6.53 (d, $J = 5.2$ Hz, 1H), 5.92 (s, 1H), 5.18 (s, 1H), 4.47–4.44 (m, 2H), 4.00–3.98 (m, 2H), 3.74–3.57 (m, 4H), 3.39 (s, 3H), 2.69–2.64 (m, 1H), 0.95–0.91 (m, 2H), 0.78–0.75 (m, 2H). ¹³C NMR (101 MHz, Chloroform-*d*) δ 212.79, 195.11, 187.58, 168.76, 168.54, 159.35, 158.44, 154.45, 127.89, 125.02, 123.14, 121.01, 108.84, 87.36, 72.76, 71.41, 70.21, 69.77, 59.13, 57.47, 23.26, 17.47, 17.25, 17.09, 7.19. HR-MS (ESI-TOF) *m/z*: calcd for C₂₅H₂₇ClN₄O₆ [M + H]⁺ 514.1619, found 515.2718. HPLC purity: 98%.

2.2. Cell lines and cell culture

The vascular endothelial cells (HUVEC), hepatocellular carcinoma cells (Hep3b2.1-7 and HepG2), colorectal cancer cells (HCT116) and immortalized normal liver cells (LO2) were purchased from Cell Bank of the Chinese Academy of Sciences (Shanghai, China). Cells were cultured in EBM-2 (Lonza, plus Single Quots Kit), RPMI-1640 (Gibco), DMEM medium (Hyclone), or MEM medium (Hyclone). The medium for all cell lines was supplemented with 10% (v/v) fetal bovine serum (FBS), penicillin (100 U/mL) and streptomycin (100 µg/mL), maintained at 37 °C in a humidified atmosphere with 5% CO₂.

2.3. Kinase inhibition assay

Kinase inhibition assay of compound ZLF-095 was performed by Eurofins (Eurofins Pharma Discovery, UK). Gradient concentration of ZLF-095 against VEGFR1-3, FGFR1-4 and PDGFR were tested. Then IC₅₀ value was calculate by GraphPad Prism software (Version 7.0, California, United States). Assay details are available on the Eurofins website (<http://www.kinhub.org/kinmap/>).

2.4. Cytotoxicity assays cytotoxicity assays

MTT assays were used to detect cytotoxic activity in different cell lines. In brief, the cells (2–5 × 10³ cells/well) were seeded in 96-well plates filled with EBM-2, RPMI-1640, DMEM, or MEM medium. After 24 h, the cells were treated with different concentration of compounds (dissolved in DMSO). After indicated time treatment, MTT solution (20 µL, 5 mg/mL) was added. After 4 h incubation, the formazan crystal formed by the living cells was dissolved with 150 µL DMSO. The absorbance was measured by a microplate spectrophotometer at 570 nm. The value of IC₅₀ was calculated by the Graphpad Prism software.

2.5. EdU staining, migration, invasion and tube formation assays of HUVECs

For EdU staining assay, 1 × 10⁴ cells were plated in 96-well plates and administrated with different concentrations of ZLF-095, Lenvatinib or the solvent control. The cells were stained with Cell-Light (TM) EdU DNA Cell Proliferation Kit (RiboBio, Guangzhou, China) and assessed by a fluorescence microscope. The evaluation metric of EdU incorporation assay is the ratio of EdU stained cells (with red fluorescence) to Hoechst33342 stained cells (with blue fluorescence).

For migration assay, HUVECs were cultured in 6-well plates and the cell surface was scratch-wounded. Then the cells were washed with PBS and treated with ZLF-095 or Lenvatinib. After incubation for 24 h, pictures were taken under microscope.

For invasion assay, the upper layer of the transwell chamber was coated with 70 µL Matrigel (BD Biosciences), then add 100 µL growth factor-free ECM medium containing 4 × 10⁴ HUVEC cells. 500 µL ECM containing various growth factors was filled to the bottom layer. The upper cells were treated with DMSO, ZLF-095 or Lenvatinib. After 24 h, the non-migrating cells were scraped off, the migrated cells were fixed with 4% paraformaldehyde, and stained with crystal violet solution and photographed under an inverted fluorescence microscope.

For HUVEC tube formation assay, 60 µL Matrigel was added to the pre-chilled 96-well plates and polymerized at 37 °C for 1 h. HUVEC cells were harvested and suspended in ECM medium was seeded on Matrigel at a density of 2 × 10⁴ cells/well with ZLF-095 or Lenvatinib. After 6 h of incubation, tube formation was observed under a microscope.

2.6. Drug studies in zebrafish

Transgenic zebrafish embryos were produced by natural spawning and distributed into 12-well plates with 10 embryos in each well, and incubated with ZLF-095, Lenvatinib or DMSO for 16 h. Imaging was performed using laser confocal microscopy (Nikon Instruments Inc.).

2.7. Colony formation assay

HCT116, Hep3B2.1-7 and HepG2 cells were seeded into 12-well plates at a density of 1.5 × 10³ cells/well. After treated with

various concentration of ZLF-095 for 10 days, the cells were fixed with 4% paraformaldehyde for 20 min and stained with 0.5% crystal violet solution for 10 min. The colonies were photographed and counted.

2.8. Western blot analysis

The cells treated with ZLF-095 or Lenvatinib at different concentrations for 48 h were harvested and lysed in RIPA buffer. The protein concentration of the supernatant was measured using a BCA Protein Assay Kit (Thermo Fisher Scientific, MA, USA). Equivalent amounts of total proteins (100 μ g) were loaded on 10% SDS-PAGE gel and transferred to nitrocellulose membranes. After blocking the NC membrane with TBST containing 5% skimmed milk powder for 2 h. The membranes were incubated with primary antibodies overnight at 4 °C and secondary antibodies for 1 h at room temperature. Lastly, membranes were visualized by employing ECL as the HRP substrate.

2.9. Flow cytometry assay

HCT116, Hep3B2.1-7 and HepG2 cells were seeded into 6-well plates with 3×10^4 cells/well and cultured for 24 h. Then the cells were treated with ZLF-095 or Lenvatinib at different concentrations for 48 h and were harvested to perform flow cytometric analysis. According to the manufacturer's instructions and relevant methods, apoptosis assay kit (keygen Biotechnology, Nanjing, China), JC1 Mitochondrial Membrane Potential Assay Kit and ROS assay kit (Beyotime Biotechnology, Jiangsu, China) were used to measure apoptosis ratio, mitochondrial membrane potential and intracellular ROS levels after ZLF-095 or Lenvatinib treatment, respectively. Then, these processes were detected by flow cytometer (Aligent NovoCyte) and quantified using NovoExpress software.

2.10. Pharmacodynamic assay of subcutaneous xenotransplantation model

All of the animal experiments were approved by the experimental animal ethics committee (Sichuan University). Balb/c female nude mice (6–8 weeks old) were purchased from Hua Fukang Experimental Animal Center (Beijing, China).

We established HCT116 xenograft models by injection HCT116 cells (5×10^6 cells in 100 μ L of PBS) subcutaneously into the right-flanks of BALB/C nude mice. When the mean tumor volume reached approximately 150 mm³ (initial tumor model) or 300 mm³ (the medium-term tumor model), the tumor-bearing mice were randomly divided into four groups (five mice per group): i. Vehicle group (control), ii. ZLF-095 5 mg/kg group, iii. ZLF-095 15 mg/kg group, iv: Lenvatinib 5 mg/kg group.

The establishment of HepG2 and Hep3B2.1-7 xenograft models were the same as HCT116 initial tumor model. The dosing regimen for HepG2 xenograft model: i. Vehicle group (control), ii. ZLF-095 50 mg/kg group, iii. Lenvatinib 30 mg/kg group. The dosing regimen for Hep3B2.1-7 xenograft model: i. Vehicle group (control), ii. ZLF-095 30 mg/kg group, iii. ZLF-095 80 mg/kg group, iv: Lenvatinib 30 mg/kg group.

Tumor volumes were measured every three days and calculated according to the following formula: Tumor volume (mm³) = $0.5 \times a \times b^2$, "a" represents length and "b" represents width). At the end of the treatment, the mice were sacrificed under anesthesia. The tumor tissues, the mouse heart, liver, spleen, lung and kidney were taken out for H&E staining and Immunohistochemistry.

2.11. Statistical analysis

GraphPad Prism 7.0 was used to perform statistical analysis. Data were presented as Means \pm SD. Comparisons of two groups were performed using a Student's *t*-test. The statistical significance in figures is represented by: **p* < 0.05, ***p* < 0.01, ****p* < 0.001.

3. Results and discussion

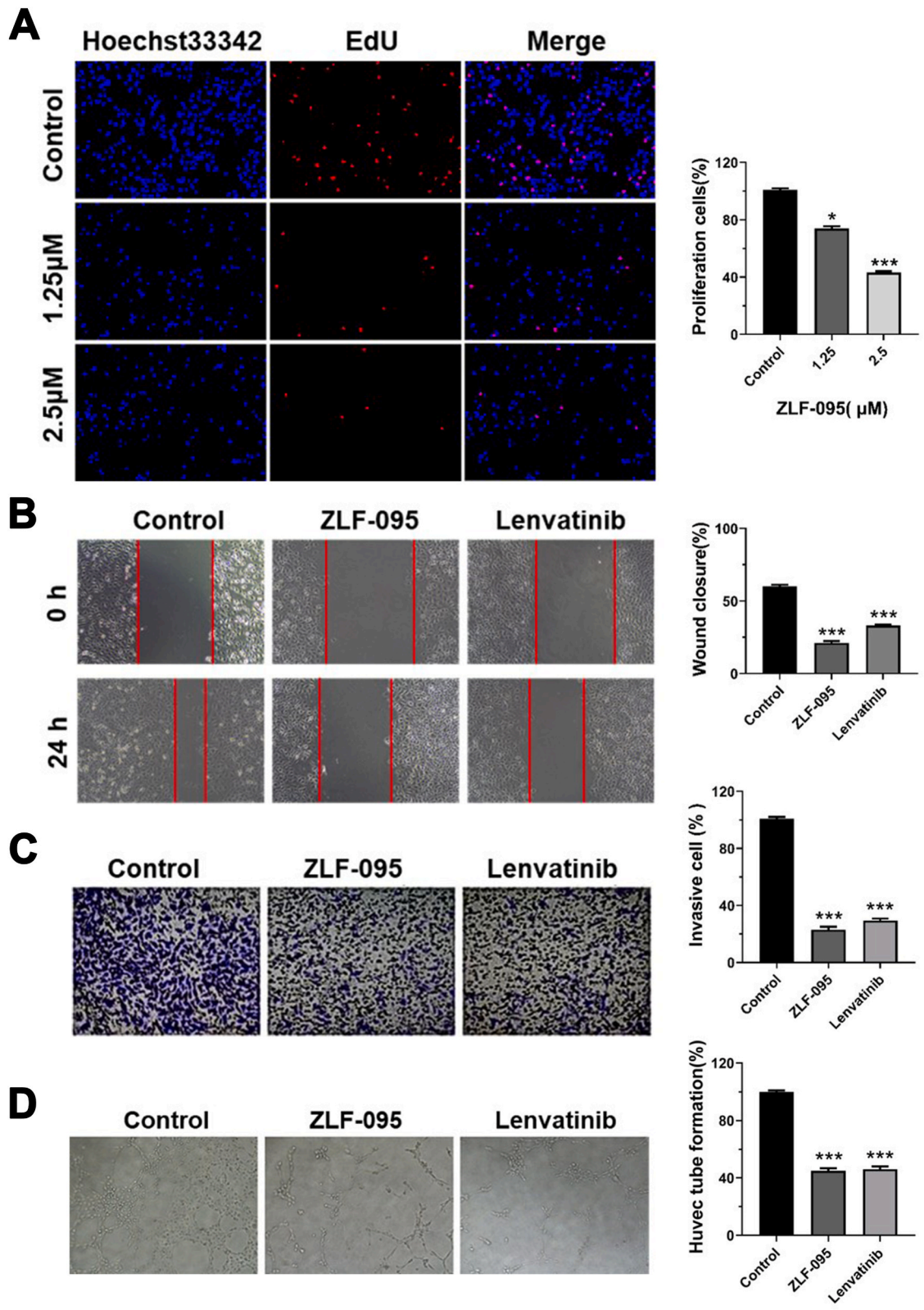
3.1. Identification of compound ZLF-095 by screening of a self-built compound library

In order to develop medicines that have more activity and less toxicity compared with Lenvatinib (Fig. 1A), we have set up a compound library of Lenvatinib analogues. According to the cocrystal structure of Lenvatinib in complex with VEGFR2 [30] (Fig. 1B), the methoxy is adjacent to the ligand binding pocket and thus may represent a suitable site to link with other groups without losing the binding affinity dramatically. According to the design principle above, we have designed and synthesized a series of compounds. ZLF-095 was chosen for further studies by screening of this self-built compound library (Fig. 1C). ZLF-095 had high activity and high selectivity for tyrosine kinases, and its IC₅₀ for VEGFR1/2/3 (IC₅₀ = 2, 5, and 0.7 nmol/L, respectively) was similar to Lenvatinib (Fig. 1D).

3.2. ZLF-095 inhibited angiogenesis in vitro and in vivo

The proliferation, migration, invasion and tube formation of vascular endothelial cells hold critical positions in the process of tumor angiogenesis [31, 32]. To evaluate the inhibitory activity of ZLF-095 on these aspects, several bioactivity assays were carried out.

MTT assay was used to assess the viability of various treatments cells. After 48 h, ZLF-095 showed more significant inhibition of VEGF165-induced HUVECs (IC₅₀ = 1.77 μ M) than untreated HUVECs (IC₅₀ = 10.07 μ M). The EdU assay further demonstrated that ZLF-095 reduced cell proliferation in VEGF165-induced HUVECs in a dose-dependent manner (Fig. 2A). Endothelial transmigration has



(caption on next page)

Fig. 2. ZLF-095 inhibits cell proliferation, migration, invasion and capillary tube formation in vitro. (A) EdU incorporation assay analysis of cell proliferation treated with ZLF-095 in HUVEC cells. (B) HUVECs cells were treated with ZLF-095 or Lenvatinib (1.25 μ M). The wound-healing assays were used for evaluating the migration abilities of the cells. (C) Images of invasive cells treated by ZLF-095 or Lenvatinib (1.25 μ M) in the transwell invasion assay. (D) ZLF-095 (3 μ M) inhibited capillary tube formation of HUVECs. All data are presented as mean \pm SD from three independent experiments (n = 3). **p < 0.01, ***p < 0.001.

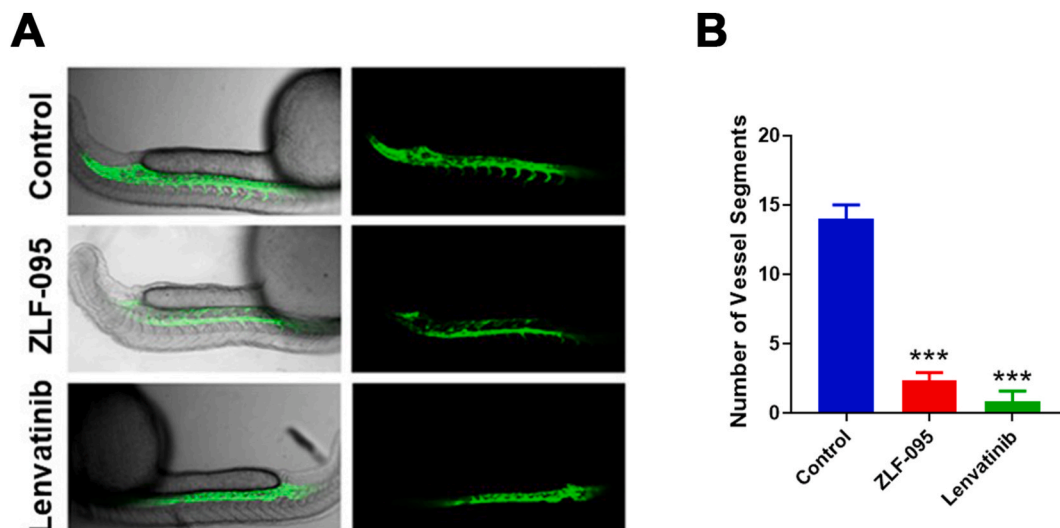


Fig. 3. ZLF-095 inhibits capillary tube formation in vivo. (A) Transgenic zebrafish was treated with DMSO, ZLF-095 or Lenvatinib (3 μ M) for 16 h, the zebrafish subintestinal vessels (SIVs) were observed using a confocal microscope. (B) The number of the zebrafish subintestinal vessels were counted. All data are presented as mean \pm SD from three independent experiments (n = 3). ***p < 0.001.

been shown to play an important role in the formation of tumor blood vessels [33]. Wound healing assay revealed that ZLF-095 inhibited the migration of HUVECs slightly better than Lenvatinib (Fig. 2B). Transwell assay was used as an evaluation of the HUVECs invasion ability under exposure to ZLF-095. As shown in Fig. 2C, ZLF-095 significantly inhibited the invasion of HUVECs, similar to Lenvatinib. Images of tube forming assay displayed that 3 μ M ZLF-095 significantly inhibited the formation of new tubes (Fig. 2D). In conclusion, ZLF-095 could significantly prevent angiogenesis in vitro by inhibiting proliferation, migration, invasion and tube formation of vascular endothelial cells.

As the inhibition effect of ZLF-095 on angiogenesis in vitro, we used flk: eGFP transgenic zebrafish as a visual model to determine whether it has the same effect in vivo [34]. Zebrafish embryos were incubated with DMSO, ZLF-095, and Lenvatinib for 16 h. Then the samples were visualized using confocal microscopy. The images revealed that ZLF-095 significantly suppressed the formation of intersegmental vessels (ISV), similar to Lenvatinib (Fig. 3A and B). In a word, ZLF-095 could significantly inhibit angiogenesis in vitro and in vivo.

3.3. ZLF-095 inhibited the VEGF2/VEGFR2 and their downstream signalling pathway

The VEGF/VEGFR signaling pathway has been considered as the major pathway for regulating angiogenesis [35–37], and VEGF2/VEGFR2 is the most important signal transducer [38–40]. The kinase inhibition assays showed that ZLF-095 significantly inhibited human VEGFRs. In order to explore the further molecular mechanism of ZLF-095, we examined its effect for the VEGF2/VEGFR2 and downstream signaling in HUVEC cells lines. As shown in Fig. 4A–G, the phosphorylation of VEGFR2 induced by 50 ng/mL VEGF-165 in HUVECs was obviously suppressed by ZLF-095 (3.3 μ M). The VEGFR2 phosphorylation leads to the activation of several downstream signalling substrates including STAT3 and ERK, thereby inducing endothelial-cell proliferation, migration, invasion and tube formation [41–45]. ZLF-095 could also significantly inhibited the STAT3 and ERK phosphorylation (1.0 and 0.3 μ M, respectively.). These results suggested that ZLF-095 mainly inhibited the phosphorylation of VEGFR2 and its downstream proteins in a dose-dependent manner.

3.4. The anti-tumor activity of ZLF-095 in vitro

In a drug candidate screening of the self-built compound library, we found that ZLF-095 notably inhibited cancer cell proliferation (Fig. 5A). To confirm its role in cancer cell proliferation, hepatocellular carcinoma cells (HepG2 and Hepa3B2.1-7) and colonic cancer cells (HCT116) were treated with different concentrations of ZLF-095, and the cell viability was analyzed by MTT assay and crystal violet staining assay. The outcomes revealed that the proliferation of these cells was significantly inhibited by ZLF-095 in a time-dependent and dose-dependent manner (Fig. 5B and C). We also employed EdU (5-ethynyl-2'-deoxyuridine) incorporation assay to

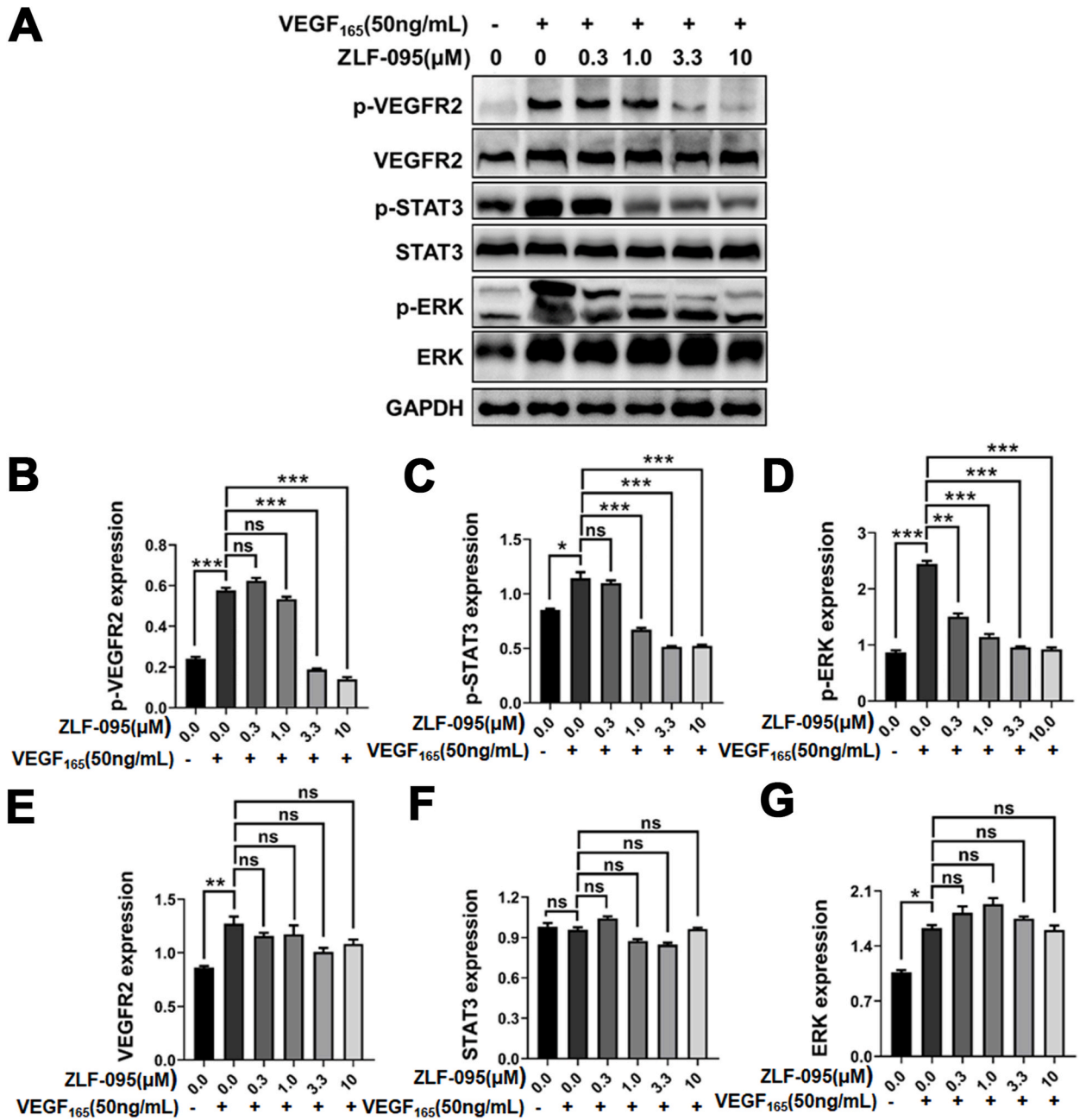
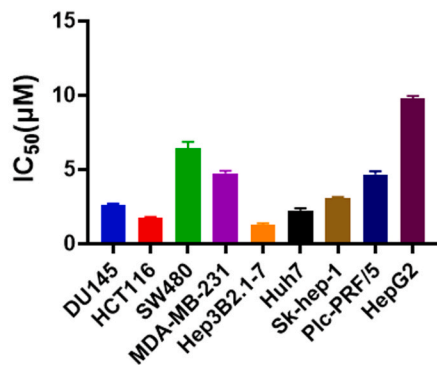
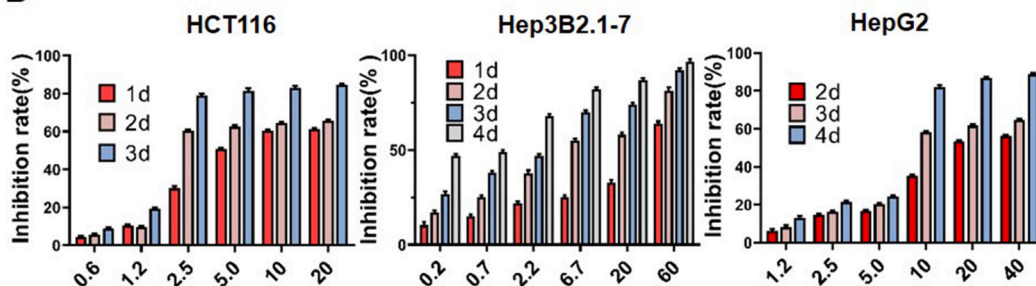


Fig. 4. ZLF-095 inhibits VEGF-VEGFR2 pathway in HUVECs. (A–G) ZLF-095 inhibited VEGF-induced phosphorylation of VEGFR2 and its downstream regulator ERK and STAT3 in HUVECs. Glyceraldehyde-3-phosphate dehydrogenase (GAPDH) was used as a loading control. Statistical analysis of All data are presented as mean ± SD from three independent experiments (n = 3). **p < 0.01, ***p < 0.001.

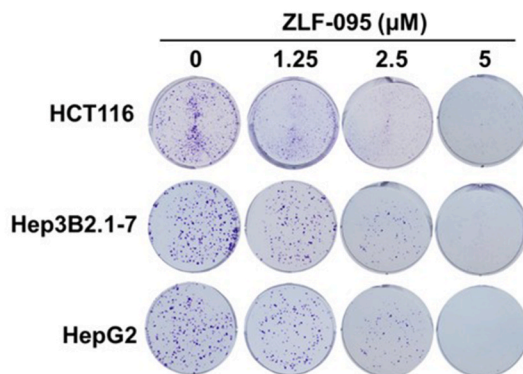
A



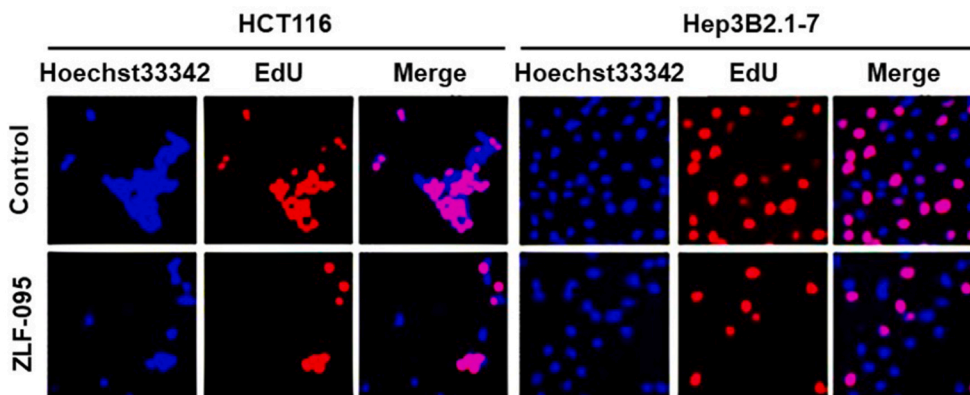
B



C



D



(caption on next page)

Fig. 5. The antiproliferative effects of ZLF-095 on various cancer cell lines. (A) The IC₅₀ value of ZLF-095 on various cancer cell lines. The liver cancer cells were treated with ZLF-095 for 6 days, and the other cells were treated for 3 days. (B) HCT116, Hep3B2.1-7 and HepG2 cells were treated with increasing doses of ZLF-095 for different time. (C) Effects of ZLF-095 on cell colony formation after treatment for 10 days. (D) Cell proliferation of HCT116 cells treated with 1 μ M ZLF-095 and Hep3B2.1-7 cells treated with 1.25 μ M ZLF-095 for 48 h were examined by EdU incorporation assay. EdU-positive (red) and Hoechst 33342 staining (blue) cells represented the proliferative and total cells, respectively. All data are presented as mean \pm SD from three independent experiments (n = 3).

assess the antiproliferative effect of ZLF-095 on HCT116 and Hep3B2.1-7 cells. Results showed that ZLF-095 significantly reduced cell proliferation (Fig. 5D). Altogether, these experiments indicated that ZLF-095 could substantially suppress the proliferation of HCT116, Hep3B2.1-7 and HepG2 cells in vitro.

3.5. ZLF-095 significantly inhibited tumors in both colorectal cancer and liver cancer xenograft models

To further evaluate the anti-tumor activity of ZLF-095 in vivo, four cancer xenograft models were established in Balb/c nude mice. We established two types of HCT116 colorectal cancer xenograft model, an initial tumor model (tumors reached volume of \sim 150 mm³) and a medium-term tumor model (tumors reached volume of \sim 300 mm³) [46,47]. Mice were orally administered with ZLF-095 at dose of 5 mg/kg and 15 mg/kg, or 5 mg/kg Lenvatinib once daily.

ZLF-095 showed remarkable tumor suppressive effects in both initial and medium-term HCT116 tumor models in a dose-dependent manner with inhibitory rates of 72.7%, 83.9%, 60.7% and 72.5%, respectively. Meanwhile, the inhibitory rates of Lenvatinib were 76.8% and 66.5% (Fig. 6A and B). In the HepG2 hepatoma xenograft model, 50 mg/kg ZLF-095 displayed significant suppression of cancer growth (75.2%) and no influence on the weight after administered for 25 days. Meanwhile, a marked loss of body weight led to death in mice occurred in 30 mg/kg Lenvatinib treatment group after 16 days (Figs. 6C and 7C). In the Hep3B2.1-7 hepatoma xenograft model, 30, 80 mg/kg ZLF-095 and 30 mg/kg Lenvatinib displayed significant inhibition with growth inhibition rates of 66.6%, 81.5% and 78.1%, respectively (Fig. 6D). Experiment was terminated on day 15 because of the sustained weight loss of the mice in Lenvatinib treatment group (Fig. 7D). These results proved that ZLF-095 was an effective inhibition for treatment of colorectal cancer and liver cancer.

To investigate the mechanisms of the antitumor effects of ZLF-095 in vivo, immunohistochemical analysis was performed on tumor tissues. As depicted in Fig. 6E, the expression of Ki67 (a cellular marker for proliferation) [48] was significantly decreased induced by ZLF-095, while the number of apoptotic cells in tumor tissues was increased compared with controls detected by TUNEL staining [49], indicating that ZLF-095 could strongly inhibit tumor growth in vivo in antiproliferation and apoptosis manner. Furthermore, we assessed the expression and distribution of vascular markers CD31 [50] to determine the antiangiogenic activity of ZLF-095 in vivo, resulting that micro-vessel density of tumors in the ZLF-095 treated groups were markedly decreased compared with controls. These findings suggested a significant antiangiogenic activity of ZLF-095 in vivo, consistent with results that ZLF-095 suppressed HUVECs proliferation in vitro and angiogenesis in zebrafish model.

3.6. ZLF-095 displayed minimal toxicity

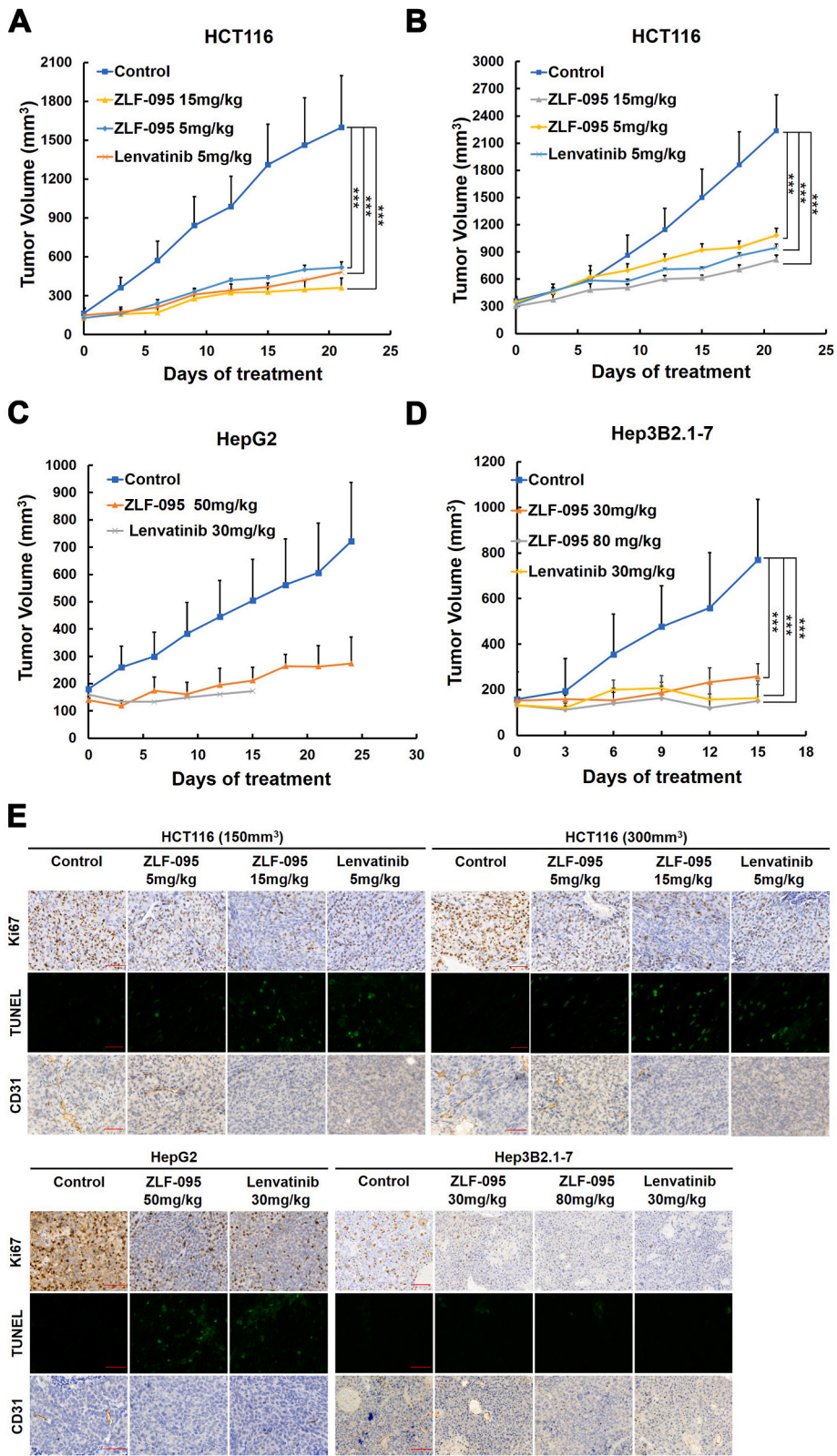
Pharmacodynamics studies revealed that ZLF-095 had significant anti-tumor activity in vivo. Most importantly, ZLF-095 treatment was well tolerated, without significant weight loss in experimental mice. In both initial and metaphases HCT116 tumor models, 5 mg/kg Lenvatinib-treated mice had lower body weights than ZLF-095-treated group (Fig. 7A and B). In HepG2 hepatoma xenograft model, 30 mg/kg Lenvatinib treatment induced acute reductions of body weight and lethality in mice, so Lenvatinib administration was stopped on day 16. In contrast, 50 mg/kg ZLF-095 treatment mice did not exhibit any significant changes in body weight nor any gross morphological abnormalities until day 25 (Fig. 7C). The same was seen in the Hep3B2.1-7 hepatoma xenograft model, no gross abnormalities were observed in ZLF-095-treated group at dose levels up to 80 mg/kg (Fig. 7D), indicating that treatment of mice with compound ZLF-095 up to 80 mg/kg was safe.

At the end of the in vivo pharmacodynamic experiments, the major organs (heart, liver, spleen, lung, and kidneys) of the mice were harvested and analyzed for histology with H&E staining [51]. No overt abnormalities were observed in these organs of all groups (Fig. 7E, F, G and H).

To further evaluated the systemic toxicity of ZLF-095, we carried out sub-acute toxicity study in vivo. Female C57BL/6 mice were orally administered with ZLF-095 (100 mg/kg) or Lenvatinib (40 mg/kg) for 25 days. As shown in Fig. 8A and B, none of the mice treated with ZLF-095 (100 mg/kg) died during the study and no significant changes in body weight was observed compared with vehicle treated mice. However, animals that received 40 mg/kg Lenvatinib showed obvious body weight loss and all the mice (5/5) died during the experiment.

Importantly, the liver images and H&E also showed that there were no visible abnormalities in the liver after 100 mg/kg ZLF-095 treatment, while 40 mg/kg Lenvatinib treated group mice showed focal necrosis and significant inflammatory cell infiltration in the liver sections p (Fig. 8C). No aberrant serum levels of BUN, CREA, GLB, UREAL, ALP, AST and ALT were detected after ZLF-095 administration (Fig. 8D and E), confirming its low toxicity to the heart, kidney and liver. ALP, AST and ALT were markers of liver injury [52,53], the notably increased levels of ALP and decreased levels of AST and ALT were observed in Lenvatinib-treated group (Fig. 8E), suggesting liver toxicity of Lenvatinib.

Collectively, these results demonstrated the low toxicity of ZLF-095 in vivo and its safety as an anticancer agent.



(caption on next page)

Fig. 6. ZLF-095 inhibits the growth of HCT116, The Hep3B2.1-7 and HepG2 xenografts in vivo. (A, B, C, D) Tumor suppression of HCT116 (150 mm³), HCT116 (300 mm³), HepG2 and Hep3B2.1-7 tumor xenografts in Balb/c nude mice treated with different concentrations of ZLF-095 or Lenvatinib. Data are presented as mean \pm SD. n = 5, ***P < 0.001. (E) Tumor tissues were immunohistochemically analyzed with anti-Ki67, TUNEL and CD31. Scale bars, 50 μ m.

3.7. ZLF-095 could mitigate the ROS-caspase3-GSDME-dependent pyroptosis in cells

We conducted investigations to explore the possible mechanisms for the lower incidence of hepatic toxicity with ZLF-095 versus Lenvatinib. MTT assay showed that Lenvatinib was toxic to the normal liver cells LO2 (IC₅₀ = 14.0 μ M) (Fig. 9A). Microscopy imaging results revealed that Lenvatinib-treated LO2 cells performed large bubbles bulging from the cell membrane, which was a typical pyroptosis cell morphology, but there was no such change was seen in ZLF-095-treated cells (Fig. 9B). We proceeded to examine whether Lenvatinib also have such effect in HCT116, Hep3B2.1-7 and HepG2 cells. Similarly, Lenvatinib could still induce pyroptosis in these cell lines. However, ZLF-095 had no such effect, and apoptotic bodies were identifiable (Fig. 9C). Next, HCT116 cells were incubated for 48 h with Lenvatinib or ZLF-095, followed by annexin V-FITC/PI double staining and to quantify annexin V-FITC positive stage and annexin V-FITC/PI double positive stage cells. The results indicated that Lenvatinib-treated cells proceeded rapidly to the annexin V-FITC/PI double-positive stage, significantly more than ZLF-095 (Fig. 9D). From these results we estimated that Lenvatinib provoked cell death mainly by inducing pyroptosis, while ZLF-095 caused antiproliferative capacity through apoptosis in HCT116, Hep3B2.1-7 and HepG2 cells.

The GSDME protein was once known as a marker of pyroptosis, as shown in Fig. 10A–D, it was positive in HCT116, Hep3B2.1-7 and HepG2 cells. The expression of N-GSDME and cleaved-caspase3 was obviously up-regulated by Lenvatinib in a concentration manner. Meanwhile, ZLF-095 led to increased caspase3 activation, but had no effect on N-GSDME protein expression. To verify the function of GSDME cleavage by caspase-3 in pyroptosis, we employed caspase 3-specific inhibitor Z-DEVD-FMK, to suppress the cleavage of caspase-3. We found that Lenvatinib-induced cell swelling was abolished by Z-DEVD-FMK (Fig. 12A). Meanwhile, the inhibition of caspase-3 Z-DEVD-FMK restrained Lenvatinib-induced generation of cleaved-caspase3 and N-GSDME (Fig. 12B). All these results suggested that Lenvatinib could provoke caspase3-GSDME-dependent pyroptosis in GSDME-expressing cells, and ZLF-095 might switch pyroptosis to apoptosis in these cells.

Recent studies have suggested mitochondrial membrane potential (MMP) imbalance and ROS accumulation contributes to the toxicity of Lenvatinib [54]. The MMP of ZLF-095 and Lenvatinib treated cells were detected after 48 h treatment by flow cytometry after staining with rhodamine 123 (Rh123). The MMP was concentration-dependently decreased by Lenvatinib in HCT116, HepG2 and Hep3B2.1-7 cells, while no significant change in MMP was seen in the ZLF-095-treated group (Fig. 11A). In addition, JC-1-labeled HCT116 cells were observed under inverted fluorescence microscopy. The green fluorescence intensity was significantly enhanced in the Lenvatinib-treated group compared to the control and ZLF-095 groups (Fig. 11C), which proved that with increasing Lenvatinib concentration, the MMP declined. These results showed that Lenvatinib could induce significant disruption of mitochondrial function.

The effects of ZLF-095 and Lenvatinib on the cellular ROS levels were also detected using flow cytometry by staining with DCFH-DA (a superoxide detection marker) after cells had been treated with ZLF-095 or Lenvatinib for 48 h. Lenvatinib significantly increased intracellular ROS levels in HCT116, HepG2 and Hep3B2.1-7 cells (Fig. 11B). Analyses of ROS using the same dye in HCT116 cells via fluorescence microscopy demonstrated a similar effect (Fig. 11D).

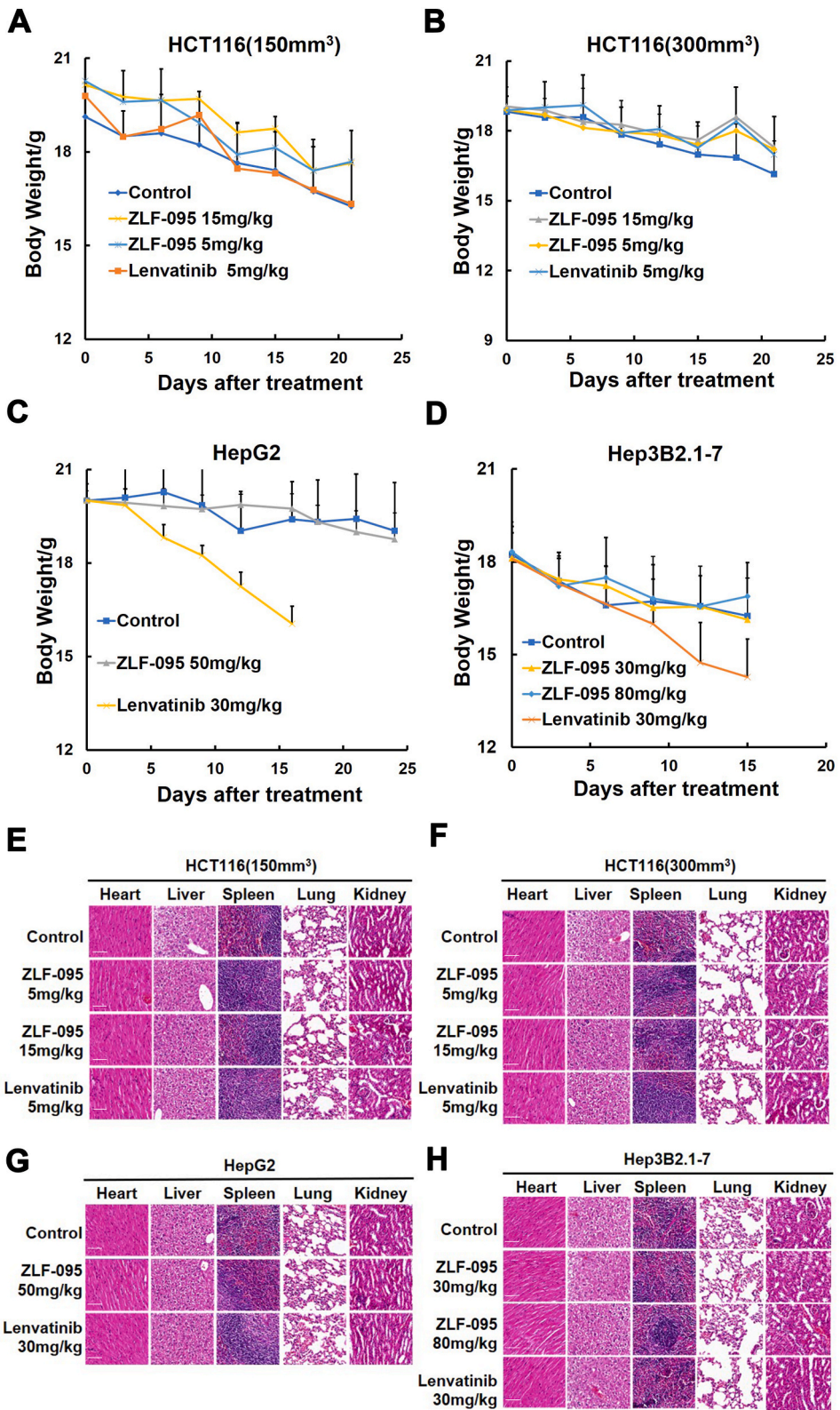
These results illustrated that Lenvatinib could trigger loss of mitochondrial membrane potential and overproduction of ROS in cells in a dose-dependent manner, while ZLF-095 may not have such effects. To evaluate the role of ROS in Lenvatinib-induced pyroptosis in GSDME-expressing cells, the ROS scavenger NAC pretreated HCT116 cells were stimulated with Lenvatinib and imaged using a microscope. The results revealed that NAC could rescue Lenvatinib-induced pyroptosis (Fig. 12A). Moreover, combined treatment with NAC and Lenvatinib reversed the cleavage of caspase 3 and GSDME (Fig. 12B).

4. Discussion

VEGF/VEGFRs promote tumor angiogenesis, leading to survival, progression, and metastasis of malignancies. Lenvatinib is an oral multi-kinase inhibitor of VEGFRs1-3, FGFR1-4, etc. It has been approved as a first-line treatment for THCA, RCC and advanced HCC. Nevertheless, adverse effects of Lenvatinib may affect its therapeutic efficacy. In order to develop a drug with higher activity and lower toxicity than Lenvatinib, the current study was conducted.

The compound ZLF-095 was selected for further study by screening a self-built library of Lenvatinib analogues. Kinase inhibition assays showed high affinity of ZLF-095 for VEGFRs and IC₅₀ for VEGFR1/2/3 at 2, 5, and 0.7 nM, respectively. This suggests ZLF-095 was a VEGFR inhibitor with great kinase inhibitory activity.

Our results validated that ZLF-095 was able to inhibit the phosphorylation of VEGFR2 and its downstream proteins, including STAT3 and ERK. At the same time, ZLF-095 was capable of inhibiting angiogenesis, migration, invasion and tube formation of vascular endothelial cells in vitro.



(caption on next page)

Fig. 7. Preliminary safety evaluation of ZLF-095 in BALB/c mice. (A, B, C, D) Body weight changes of HCT116 (150 mm³), HCT116 (300 mm³), HepG2 and Hep3B2.1-7 tumor xenografts. Data are presented as mean \pm SD (n = 5), *P < 0.05, **P < 0.01, and ***P < 0.001. (E, F, G, H) The major organs (heart, liver, spleen, lung, and kidneys) of the mice from HCT116 (150 mm³), HCT116 (300 mm³), HepG2 and Hep3B2.1-7 tumor xenografts were harvested and analyzed for histology with H&E staining. Scale bars, 50 μ m, \times 20 for micrograph.

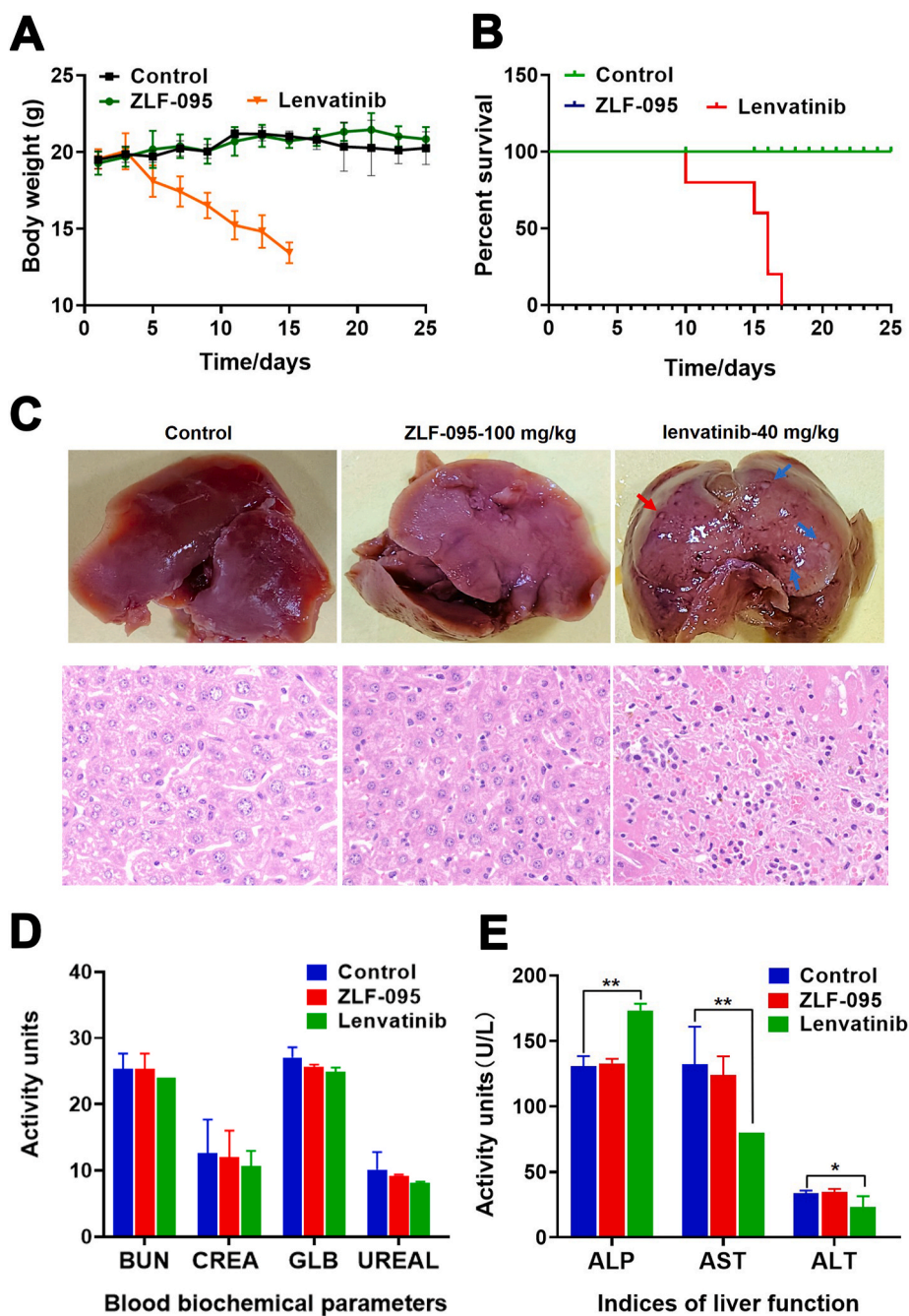


Fig. 8. Compound ZLF-095 shows low systemic toxicity. C57BL/6 mice (female) were orally administered with Vehicle, ZLF-095 (100 mg/kg), or Lenvatinib (40 mg/kg), respectively. (A) Body weights of compound ZLF-095- or Lenvatinib-treated mice. (B) Survival curves of mice. (C) Liver images and H&E staining (Scale bars, 50 μ m, \times 20 for micrograph) of livers from these groups of mice. (D, E) Plasma levels of BUN, CREA, GLB, UREAL, ALP, AST and ALT. Plasma was isolated from ZLF-095 or Lenvatinib treatment of mice. Data are presented as mean \pm SD (n = 3), *P < 0.05, **P < 0.01.

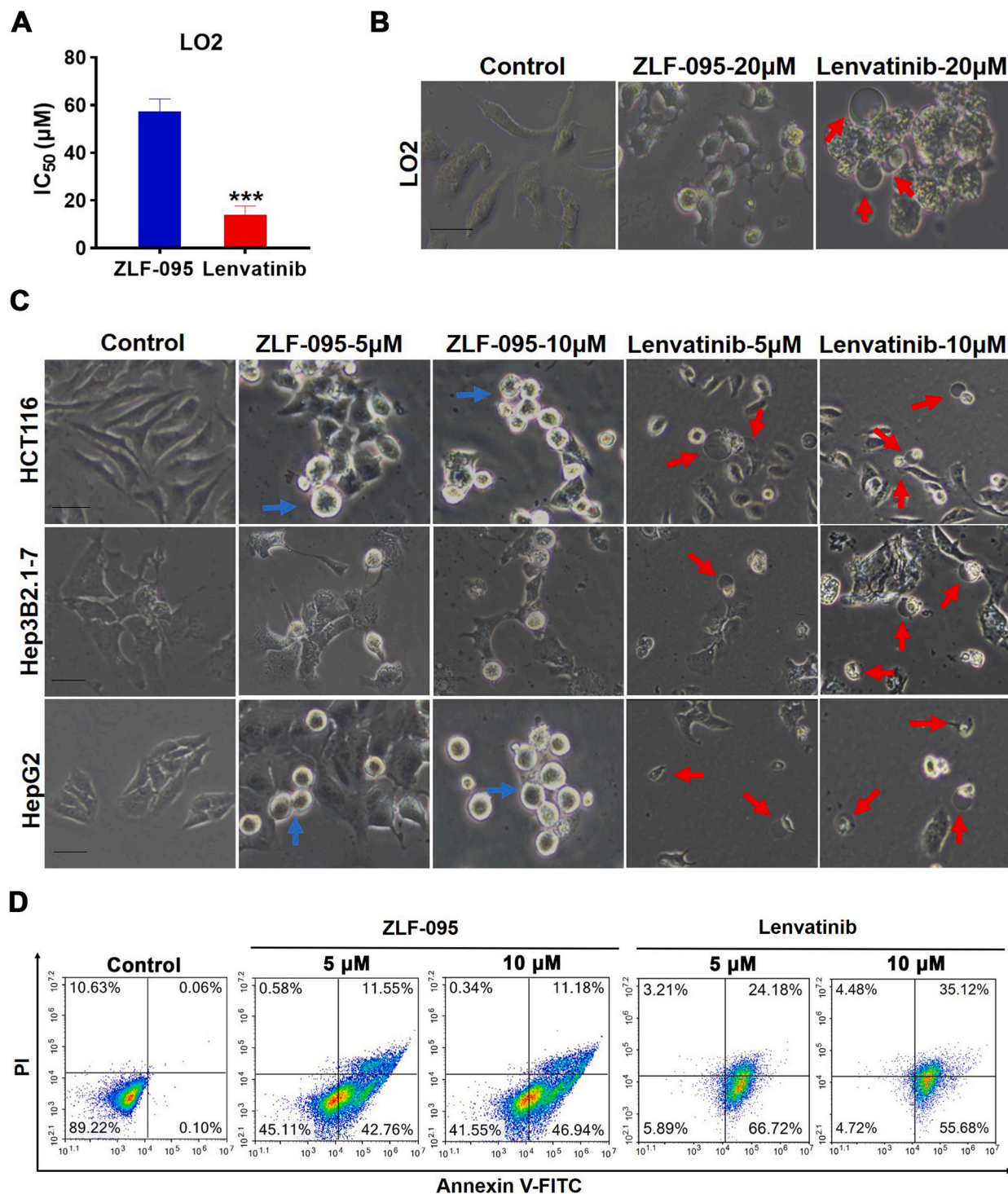


Fig. 9. Lenvatinib triggers pyroptosis in LO2, HCT116, Hep3B2.1-7 and HepG2 cells. (A) Viability across normal hepatic cell LO2 treated with ZLF-095 or Lenvatinib for 3 days was assessed. (B, C) LO2, HCT116, Hep3B2.1-7 and HepG2 cells were treated with ZLF-095 or Lenvatinib for 48 h. Microscopy imaging was performed. Blue arrows refer to apoptotic bodies, red arrows refer to ballooned cell membrane characteristic of pyroptotic cells. Scale bar, 100 μm. (D) HCT116 cells were treated with different concentrations of ZLF-095 or Lenvatinib for 48 h, stained by annexin V-FITC/PI, and analyzed by flow cytometry.

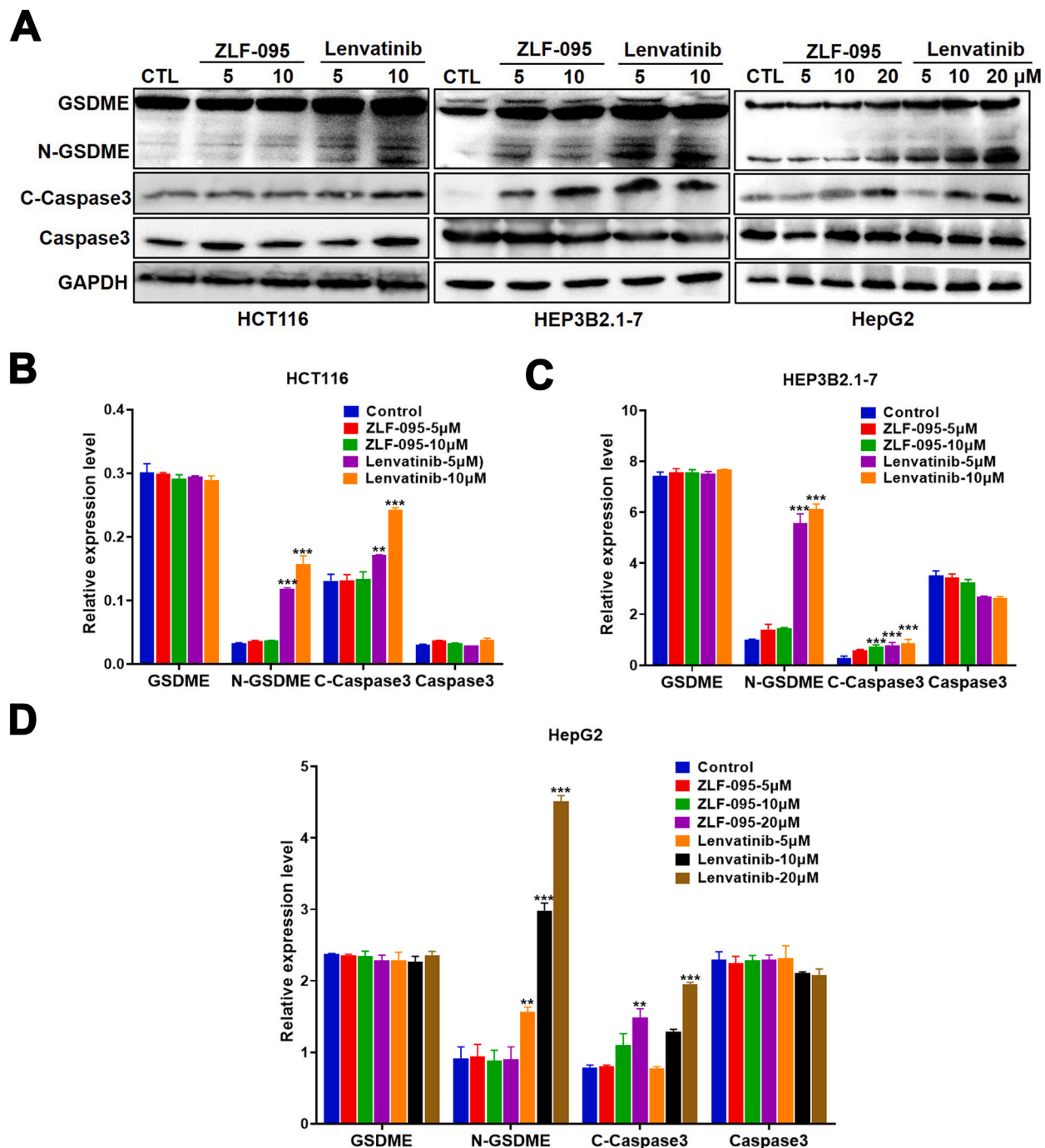
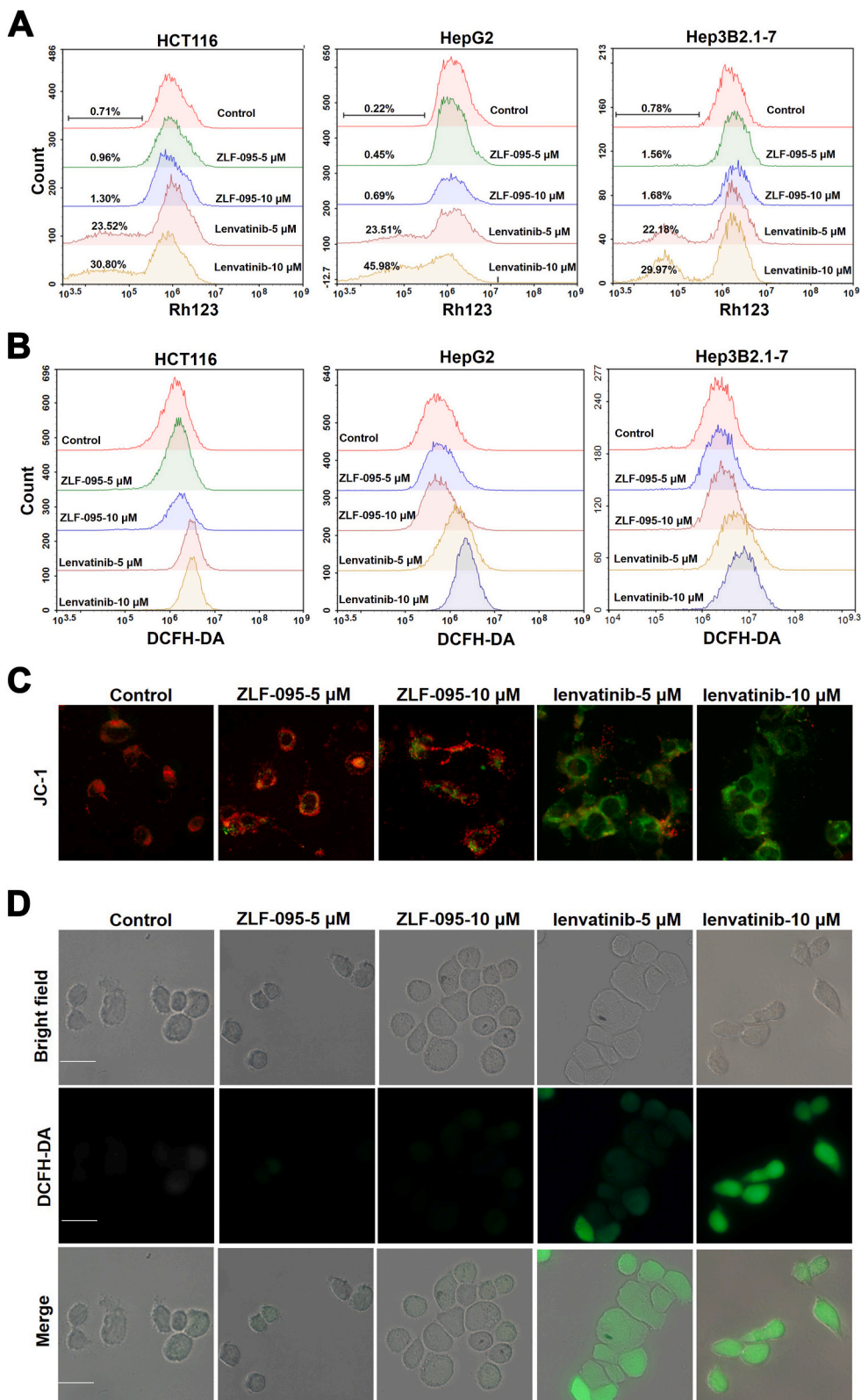


Fig. 10. Lenvatinib induces cleavage of GSDME in HCT116, Hep3B2.1-7 and HepG2 cells. (A–D) The cells were treated with ZLF-095 or Lenvatinib for 48 h, the levels of pyroptosis-related proteins (including GSDME, N-GSDME, cleaved caspase3 and caspase3) were detected. Quantification was expressed as the ratio to GAPDH. All data are presented as mean \pm SD from three independent experiments ($n = 3$). ** $P < 0.01$, and *** $P < 0.001$.



(caption on next page)

Fig. 11. Lenvatinib triggers loss of mitochondrial membrane potential and overproduction of ROS in HCT116, Hep3B2.1-7 and HepG2 cells. (A) The mitochondrial membrane potential was evaluated by flow cytometry after staining with Rh123. (B) The cellular ROS level was detected using flow cytometry by staining with DCFH-DA. (C) The fluorescence intensity of JC-1-labeled HCT116 cells under an inverted fluorescence microscope. Red fluorescence was produced when the MMP was higher, and green fluorescence was produced when the MMP was lower. Scale bar, 100 μ m. (D) Cellular ROS levels were detected by an inverted fluorescence microscopy in DCFH-DA stained HCT116 cells, green fluorescence was produced when the ROS was higher. Scale bar, 100 μ m.

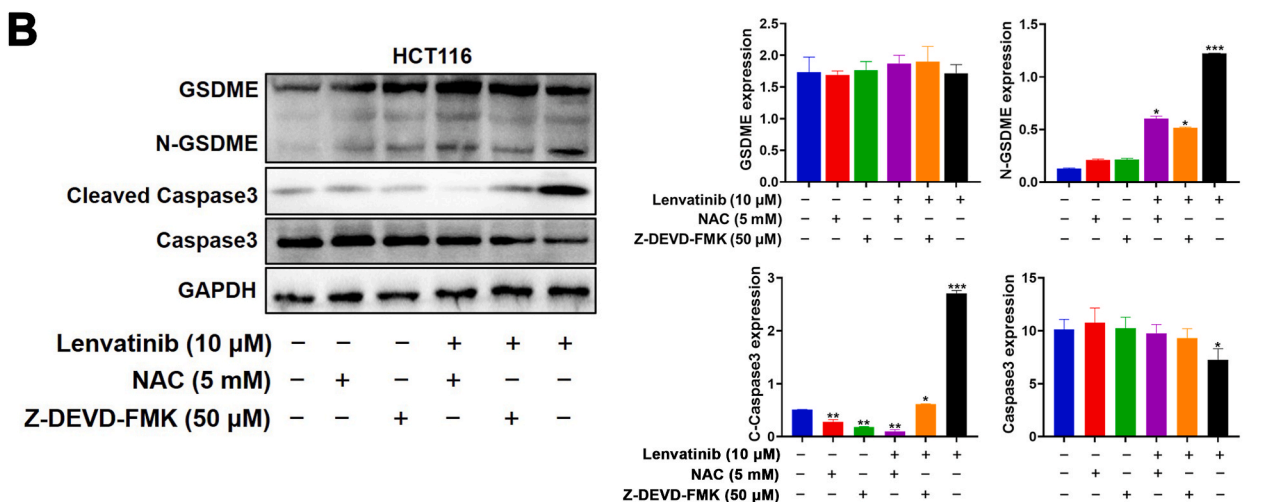
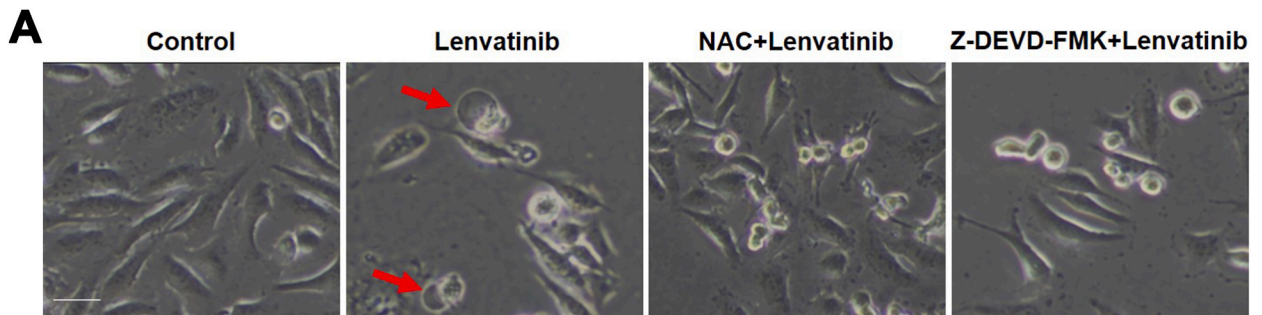


Fig. 12. NAC and Z-DEVD-FMK decreases Lenvatinib-induced pyroptosis in HCT116 cells. (A) the ROS scavenger NAC and the caspase 3-specific inhibitor Z-DEVD-FMK pretreated HCT116 cells were stimulated with Lenvatinib and imaged using a microscope. Scale bars, 100 μ m. (B) HCT116 cells in the presence or absence of NAC and Z-DEVD-FMK. All data are presented as mean \pm SD from three independent experiments (n = 3).

Then, we tested the anti-proliferative effects of ZLF-095 on multiple HCC and CC cell lines and found that it apparently inhibited cancer cell proliferation. More importantly, ZLF-095 significantly inhibited HCT116, Hep3B2.1-7 and HepG2 tumor growth, angiogenesis and metastasis in a dose-dependent manner in vivo, and demonstrated less toxicity than Lenvatinib.

In addition, we found that Lenvatinib provoked pyroptosis in LO2, HCT116, Hep3B2.1-7 and HepG2 cells, while ZLF-095 triggered apoptosis in these cell lines. Pyroptosis may induce rapid cell-membrane rupture and the release of intracellular contents, resulting in fever, hepatotoxicity, septicemia and other severe symptoms. This may be one of the reasons for the toxicity of Lenvatinib.

Finally, we verified that loss of mitochondrial membrane potential and overproduction of ROS were triggered by Lenvatinib in the HCT116, Hep3B2.1-7 and HepG2 cell lines, while ZLF-095 had no such effect. Based on these results, we speculated that Lenvatinib diminishes mitochondrial membrane potential and consequently triggers ROS-caspase3-GSDME-dependent pyroptosis in GSDME-expressing cells (HCT116, Hep3B2.1-7 and HepG2 cells), which may cause substantial inflammation and toxic side effects of drugs. Conversely, ZLF-095 had no effect on mitochondrial membrane potential and therefore could not cause ROS-caspase3-GSDME-dependent pyroptosis, thus successfully avoiding unwanted side effects (Fig. 13).

Taken together, all of these studies support ZLF-095 as a novel VEGFR inhibitor for the treatment of diverse solid tumors that deserves further investigation and development.

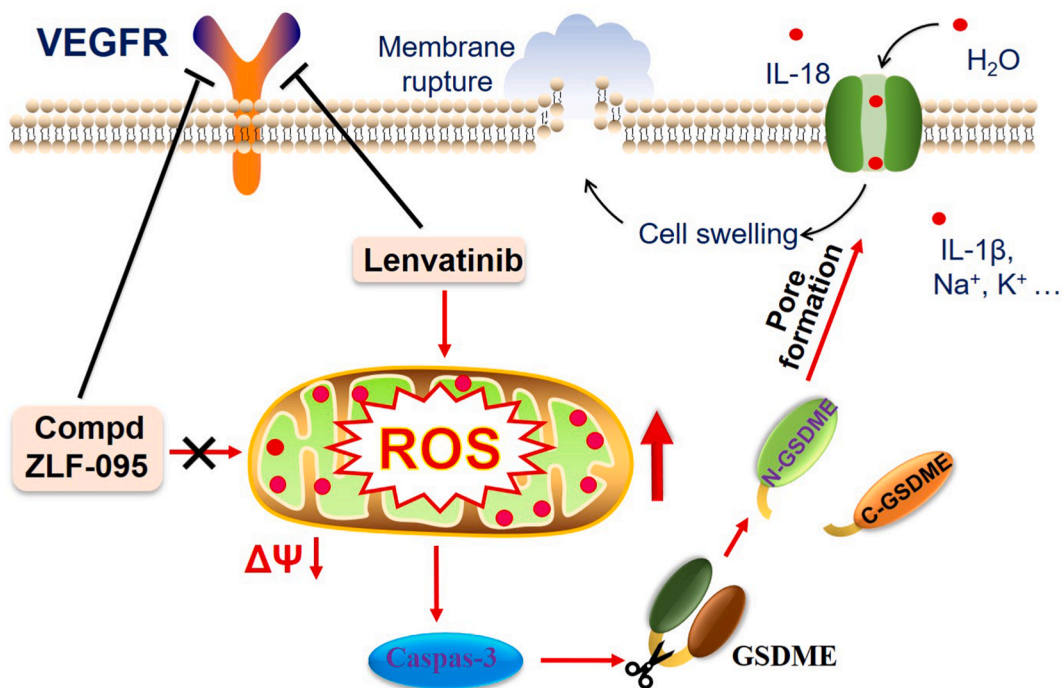


Fig. 13. ZLF-095 mitigates the ROS-caspase3-GSDME-dependent pyroptosis in GSDME-expressing cells.

Author contribution statement

Lifeng Zhao; Lidan Zhang; Luoting Yu: Conceived and designed the experiments.

Xiao Li; Jia Wang: Performed the experiments; Analyzed and interpreted the data; Wrote the paper.

Qianqian Wang; Xiaojie Song: Performed the experiments.

Tianwen Luo; Guoquan Wan; Zhanzhan Feng; Xiaojie He; Qian Lei; Ying Xu; Xinyu You: Contributed reagents, materials, analysis tools or data.

Data availability statement

Data will be made available on request.

Declaration of interest's statement

The authors declare no competing interests.

Acknowledgements

This study was supported by Sichuan Science and Technology Program (NO : 2019YFH0054). We thank Professor Tinghong Ye for the guidance provided during the study.

Appendix A. Supplementary data

Supplementary data to this article can be found online at <https://doi.org/10.1016/j.heliyon.2023.e15152>.

References

- [1] J. Folkman, M. Bach, J.W. Rowe, F. Davidoff, P. Lambert, C. Hirsch, A. Goldberg, H.H. Hiatt, J. Glass, E. Henshaw, Tumor angiogenesis - therapeutic implications, *N. Engl. J. Med.* 285 (21) (1971) 1182. WOS:A1971K841500008.
- [2] N. Weidner, J.P. Semple, W.R. Welch, J. Folkman, Tumor angiogenesis and metastasis - correlation in invasive breast-carcinoma, *N. Engl. J. Med.* 324 (1) (1991) 1-8, <https://doi.org/10.1056/nejm199101033240101>.

- [3] J. Folkman, Angiogenesis in cancer, vascular, rheumatoid and other disease, *Nat. Med.* 1 (1) (1995) 27–31, <https://doi.org/10.1038/nm0195-27>.
- [4] P. Carmeliet, R.K. Jain, Angiogenesis in cancer and other diseases, *Nature* 407 (6801) (2000) 249–257, <https://doi.org/10.1038/35025220>.
- [5] P. Carmeliet, Angiogenesis in health and disease, *Nat. Med.* 9 (6) (2003) 653–660, <https://doi.org/10.1038/nm0603-653>.
- [6] W. Risau, Mechanisms of angiogenesis, *Nature* 386 (6626) (1997) 671–674, <https://doi.org/10.1038/386671a0>.
- [7] I. Zuzazo-Gaztelu, O. Casanovas, Unraveling the role of angiogenesis in cancer ecosystems, *Front. Oncol.* 8 (2018), <https://doi.org/10.3389/fonc.2018.00248>.
- [8] A.W. Moawad, J. Szklaruk, C. Lall, K.J. Blair, A.O. Kaseb, A. Kamath, S.A. Rohren, K.M. Elsayes, Angiogenesis in hepatocellular carcinoma; pathophysiology, targeted therapy, and role of imaging, *J. Hepatocell. Carcinoma* 7 (2020) 77–89, <https://doi.org/10.2147/jhc.S224471>.
- [9] C.S. Melnicovici, A.B. Bosca, S. Susman, M. Marginean, C. Mihu, M. Istrate, I.-M. Moldovan, A.L. Roman, C.M. Mihu, Vascular endothelial growth factor (VEGF) - key factor in normal and pathological angiogenesis, *Rom. J. Morphol. Embryol.* 59 (2) (2018) 455–467. Go to ISI>://WOS:000444860300004.
- [10] R.S. Apte, D.S. Chen, N. Ferrara, VEGF in signaling and disease: beyond discovery and development, *Cell* 176 (6) (2019) 1248–1264, <https://doi.org/10.1016/j.cell.2019.01.021>.
- [11] G. Neufeld, T. Cohen, S. Gengrinovitch, Z. Poltorak, Vascular endothelial growth factor (VEGF) and its receptors, *Faseb. J.* 13 (1) (1999) 9–22, <https://doi.org/10.1096/fasebj.13.1.9>.
- [12] K.J. Kim, B. Li, J. Winer, M. Armanini, N. Gillett, H.S. Phillips, N. Ferrara, Inhibition of vascular endothelial growth factor-induced angiogenesis suppresses tumor-growth in vivo, *Nature* 362 (6423) (1993) 841–844, <https://doi.org/10.1038/362841a0>.
- [13] N. Ferrara, T. Davissmyth, The biology of vascular endothelial growth factor, *Endocr. Rev.* 18 (1) (1997) 4–25, <https://doi.org/10.1210/er.18.1.4>.
- [14] N. Ferrara, H.P. Gerber, J. Lecouter, The biology of VEGF and its receptors, *Nat. Med.* 9 (6) (2003) 669–676, <https://doi.org/10.1038/nm0603-669>.
- [15] Y. Itatani, K. Kawada, T. Yamamoto, Y. Sakai, Resistance to anti-angiogenic therapy in cancer-alterations to anti-VEGF pathway, *Int. J. Mol. Sci.* 19 (4) (2018), <https://doi.org/10.3390/ijms19041232>.
- [16] T. Li, G. Kang, T. Wang, H. Huang, Tumor angiogenesis and anti-angiogenic gene therapy for cancer (Review), *Oncol. Lett.* 16 (1) (2018) 687–702, <https://doi.org/10.3892/ol.2018.8733>.
- [17] D. Ribatti, A. Vacca, New insights in anti-angiogenesis in multiple myeloma, *Int. J. Mol. Sci.* 19 (7) (2018), <https://doi.org/10.3390/ijms19072031>.
- [18] C.C. Estrada, A. Maldonado, S.K. Mallipattu, Therapeutic inhibition of VEGF signaling and associated nephrotoxicities, *J. Am. Soc. Nephrol.* 30 (2) (2019) 187–200, <https://doi.org/10.1681/asn.2018080853>.
- [19] A. Fallah, A. Sadeghinia, H. Kahroba, A. Samadi, H.R. Heidari, B. Bradaran, S. Zeinali, O. Molavi, Therapeutic targeting of angiogenesis molecular pathways in angiogenesis-dependent diseases, *Biomed. Pharmacother.* 110 (2019) 775–785, <https://doi.org/10.1016/j.biopha.2018.12.022>.
- [20] R.I. Teleanu, C. Chircov, A.M. Grumezescu, D.M. Teleanu, Tumor angiogenesis and anti-angiogenic strategies for cancer treatment, *J. Clin. Med.* 9 (1) (2020), <https://doi.org/10.3390/jcm9010084>.
- [21] M. Kudo, Lenvatinib may drastically change the treatment landscape of hepatocellular carcinoma, *Liver Cancer* 7 (1) (2018) 1–19, <https://doi.org/10.1159/000487148>.
- [22] M. Kudo, R.S. Finn, S. Qin, K.-H. Han, K. Ikeda, F. Piscaglia, A. Baron, J.-W. Park, G. Han, J. Jassem, J.F. Blanc, A. Vogel, D. Komov, T.R.J. Evans, C. Lopez, C. Dutcus, M. Guo, K. Saito, S. Kraljevic, T. Tamai, et al., Lenvatinib versus sorafenib in first-line treatment of patients with unresectable hepatocellular carcinoma: a randomised phase 3 non-inferiority trial, *Lancet* 391 (10126) (2018) 1163–1173, [https://doi.org/10.1016/s0140-6736\(18\)30207-1](https://doi.org/10.1016/s0140-6736(18)30207-1).
- [23] M. Kudo, K. Ueshima, S. Chan, T. Minami, H. Chishina, T. Aoki, M. Takita, S. Hagiwara, Y. Minami, H. Ida, M. Takenaka, T. Sakurai, T. Watanabe, M. Morita, C. Ogawa, Y. Wada, M. Ikeda, H. Ishii, N. Izumi, N. Nishida, Lenvatinib as an initial treatment in patients with intermediate-stage hepatocellular carcinoma beyond up-to-seven criteria and child-pugh A liver function: a proof-of-concept study, *Cancers* 11 (8) (2019), <https://doi.org/10.3390/cancers11081084>.
- [24] A. Hiraoka, T. Kumada, K. Kariyama, K. Takaguchi, M. Atsukawa, E. Itobayashi, K. Tsuji, K. Tajiri, M. Hirooka, N. Shimada, H. Shibata, T. Ishikawa, H. Ochi, T. Tada, H. Toyoda, K. Nouso, A. Tsutsui, N. Itokawa, M. Imai, K. Joko, et al., Clinical features of lenvatinib for unresectable hepatocellular carcinoma in real-world conditions: multicenter analysis, *Cancer Med.* 8 (1) (2019) 137–146, <https://doi.org/10.1002/cam4.1909>.
- [25] A. Hiraoka, T. Kumada, K. Kariyama, K. Takaguchi, E. Itobayashi, N. Shimada, K. Tajiri, K. Tsuji, T. Ishikawa, H. Ochi, M. Hirooka, A. Tsutsui, H. Shibata, T. Tada, H. Toyoda, K. Nouso, K. Joko, Y. Hiasa, K. Michitaka, Real-Life Practice Experts HCC, et al. Therapeutic potential of lenvatinib for unresectable hepatocellular carcinoma in clinical practice: multicenter analysis, *Hepatol. Res.* 49 (1) (2019) 111–117, <https://doi.org/10.1111/hepr.13243>.
- [26] V. Makker, D. Rasco, N.J. Vogelzang, M.S. Brose, A.L. Cohn, J. Mier, C. Di Simone, D.M. Hyman, D.E. Stepan, C.E. Dutcus, E.V. Schmidt, M. Guo, P. Sachdev, R. Shumaker, C. Aghajanian, M. Taylor, Lenvatinib plus pembrolizumab in patients with advanced endometrial cancer: an interim analysis of a multicentre, open-label, single-arm, phase 2 trial, *Lancet Oncol.* 20 (5) (2019) 711–718, [https://doi.org/10.1016/s1470-2045\(19\)30020-8](https://doi.org/10.1016/s1470-2045(19)30020-8).
- [27] J. Shi, W. Gao, F. Shao, Pyroptosis: gasdermin-mediated programmed necrotic cell death, *Trends Biochem. Sci.* 42 (4) (2017) 245–254, <https://doi.org/10.1016/j.tibs.2016.10.004>.
- [28] Y. Wang, W. Gao, X. Shi, J. Ding, W. Liu, H. He, K. Wang, F. Shao, Chemotherapy drugs induce pyroptosis through caspase-3 cleavage of a gasdermin, *Nature* 547 (7661) (2017) 99, <https://doi.org/10.1038/nature22393>.
- [29] Q. Wang, Y. Wang, J. Ding, C. Wang, X. Zhou, W. Gao, H. Huang, F. Shao, Z. Liu, A bioorthogonal system reveals antitumor immune function of pyroptosis, *Nature* 579 (7799) (2020) 421, <https://doi.org/10.1038/s41586-020-2079-1>.
- [30] M. Mctigue, B.W. Murray, J.H. Chen, Y.L. Deng, J. Solowiej, Kania RSJPTNaOSOTUSOA. Molecular conformations, interactions, and properties associated with drug efficiency and clinical performance among VEGFR TK inhibitors, *Proc. Natl. Acad. Sci. USA* 109 (45) (2012) 18281–18289.
- [31] P. Carmeliet, R.K. Jain, Molecular mechanisms and clinical applications of angiogenesis, *Nature* 473 (7347) (2011) 298–307, <https://doi.org/10.1038/nature10144>.
- [32] S.M. Weis, D.A. Cheresh, Tumor angiogenesis: molecular pathways and therapeutic targets, *Nat. Med.* 17 (11) (2011) 1359–1370, <https://doi.org/10.1038/nm.2537>.
- [33] S. Guo, J. Lok, Y. Liu, K. Hayakawa, W. Leung, C. Xing, X. Ji, E.H. Lo, Assays to examine endothelial cell migration, tube formation, and gene expression profiles, *Methods Mol. Biol.* 1135 (2014) 393–402, https://doi.org/10.1007/978-1-4939-0320-7_32.
- [34] P. Blezinger, J. Wang, M. Gondo, A. Quezada, D. Mehrens, M. French, A. Singhal, S. Sullivan, A. Rolland, R.J.N.B. Ralston, Systemic inhibition of tumor growth and tumor metastases by intramuscular administration of the endostatin gene, *Nat. Biotechnol.* 17 (4) (1999) 343.
- [35] B. Sitohy, J.A. Nagy, H.F. Dvorak, Anti-VEGF/VEGFR therapy for cancer: reassessing the target, *Cancer Res.* 72 (8) (2012) 1909–1914, <https://doi.org/10.1158/0008-5472.Can-11-3406>.
- [36] M. Shibuya, Vascular endothelial growth factor and its receptor system: physiological functions in angiogenesis and pathological roles in various diseases, *J. Biochem.* 153 (1) (2013) 13–19, <https://doi.org/10.1093/jb/mvs136>.
- [37] R.R. Ramjiawan, A.W. Griffioen, D.G. Duda, Anti-angiogenesis for cancer revisited: is there a role for combinations with immunotherapy? *Angiogenesis* 20 (2) (2017) 185–204, <https://doi.org/10.1007/s10456-017-9552-y>.
- [38] Y. Zhao, A.A. Adjei, Targeting angiogenesis in cancer therapy: moving beyond vascular endothelial growth factor, *Oncol.* 20 (6) (2015) 660–673, <https://doi.org/10.1634/theoncologist.2014-0465>.
- [39] J. Yang, J. Yan, B. Liu, Targeting veGF/veGFR to Modulate Antitumor immunity, *Front. Immunol.* 9 (2018), <https://doi.org/10.3389/fimmu.2018.00978>.
- [40] R. Tamura, T. Tanaka, Y. Akasaki, Y. Murayama, K. Yoshida, H. Sasaki, The role of vascular endothelial growth factor in the hypoxic and immunosuppressive tumor microenvironment: perspectives for therapeutic implications, *Med. Oncol.* 37 (1) (2020), <https://doi.org/10.1007/s12032-019-1329-2>.
- [41] S.A. Lang, P. Schachtschneider, C. Moser, A. Mori, C. Hackl, A. Gaumann, D. Batt, H.J. Schlitt, E.K. Geissler, O. Stoeltzing, Dual targeting of Raf and VEGF receptor 2 reduces growth and metastasis of pancreatic cancer through direct effects on tumor cells, endothelial cells, and pericytes, *Mol. Cancer Therapeut.* 7 (11) (2008) 3509–3518, <https://doi.org/10.1158/1535-7163.Mct-08-0373>.
- [42] X. Zhang, Y. Song, Y. Wu, Y. Dong, L. Lai, J. Zhang, B. Lu, F. Dai, L. He, M. Liu, Z. Yi, Indirubin inhibits tumor growth by antitumor angiogenesis via blocking VEGFR2-mediated JAK/STAT3 signaling in endothelial cell, *Int. J. Cancer* 129 (10) (2011) 2502–2511, <https://doi.org/10.1002/ijc.25909>.
- [43] H. Lee, H.-J. Lee, I.J. Bae, J.J. Kim, S.-H. Kim, Inhibition of STAT3/VEGF/CDK2 axis signaling is critically involved in the antiangiogenic and apoptotic effects of arsenic herbal mixture PROS in non-small lung cancer cells, *Oncotarget* 8 (60) (2017) 101771–101783, <https://doi.org/10.18632/oncotarget.21973>.

- [44] Z. Wang, J.A. Li, W.A. Xiao, J. Long, H. Zhang, The STAT3 inhibitor S3I-201 suppresses fibrogenesis and angiogenesis in liver fibrosis, *Lab. Invest.* 98 (12) (2018) 1600–1613, <https://doi.org/10.1038/s41374-018-0127-3>.
- [45] W. Wang, Y. Liu, L. You, M. Sun, C. Qu, X. Dong, X. Yin, J. Ni, Inhibitory effects of Paris saponin I, II, VI and VII on HUVEC cells through regulation of VEGFR2, PI3K/AKT/mTOR, Src/eNOS, PLC gamma/ERK/MERK, and JAK2-STAT3 pathways, *Biomed. Pharmacother.* 131 (2020), <https://doi.org/10.1016/j.biopha.2020.110750>.
- [46] V. Schmitz, L. Tirado-Ledo, K. Tiemann, E. Raskopf, T. Heinicke, C. Ziske, M.A. Gonzalez-Carmona, C. Rabe, N. Wernert, J. Prieto, C. Qian, T. Sauerbruch, W. H. Caselmann, Establishment of an orthotopic tumour model for hepatocellular carcinoma and non-invasive in vivo tumour imaging by high resolution ultrasound in mice, *J. Hepatol.* 40 (5) (2004) 787–791, <https://doi.org/10.1016/j.jhep.2004.01.010>.
- [47] E. Fujii, M. Suzuki, K. Matsubara, M. Watanabe, Y.J. Chen, K. Adachi, Y. Ohnishi, M. Tanigawa, M. Tsuchiya, N. Tamaoki, Establishment and characterization of in vivo human tumor models in the NOD/SCID/gamma(null)(c) mouse, *Pathol. Int.* 58 (9) (2008) 559–567, <https://doi.org/10.1111/j.1440-1827.2008.02271.x>.
- [48] H.S. Dreja, J. Ayton, D. Bruce, J. Lochead, S. Renshaw, L. Parton, B. Hamilton, S. Beer, M. Munro, A. Solache, Knockout validation of antibodies to Ki67: a marker for cellular proliferation, *J. Immunol.* 198 (1) (2017). Go to ISI>://WOS:000407750400951.
- [49] C. Charriaumarlangue, Y. Benari, A cautionary note on the use of the TUNEL stain to determine apoptosis, *Neuroreport* 7 (1) (1995) 61–64, <https://doi.org/10.1097/00001756-199512290-00014>.
- [50] M. Miettinen, A.E. Lindenmayer, A. Chaubal, Endothelial-cell markers cd31, cd34, and bnh9 antibody to h-antigen and y-antigen - evaluation of their specificity and sensitivity in the diagnosis of vascular tumors and comparison with von-willebrand-factor, *Mod. Pathol.* 7 (1) (1994) 82–90. Go to ISI>://WOS: A1994NF42600018.
- [51] TaA. Tosta, P.R. De Faria, L.A. Neves, M.Z. Do Nascimento, Computational normalization of H&E-stained histological images: progress, challenges and future potential, *Artif. Intell. Med.* 95 (2019) 118–132, <https://doi.org/10.1016/j.artmed.2018.10.004>.
- [52] S.K. Ramaiah, A toxicologist guide to the diagnostic interpretation of hepatic biochemical parameters, *Food Chem. Toxicol.* 45 (9) (2007) 1551–1557, <https://doi.org/10.1016/j.fct.2007.06.007>.
- [53] J. Ozer, M. Ratner, M. Shaw, W. Bailey, S. Schomaker, The current state of serum biomarkers of hepatotoxicity, *Toxicology* 245 (3) (2008) 194–205, <https://doi.org/10.1016/j.tox.2007.11.021>.
- [54] A.G. Akyildiz, T. Boran, A.T. Jannuzzi, B. Alpertunga, Mitochondrial dynamics imbalance and mitochondrial dysfunction contribute to the molecular cardiotoxic effects of lenvatinib, *Toxicol. Appl. Pharmacol.* (2021) 423, <https://doi.org/10.1016/j.taap.2021.115577>.